A genetically-encoded fluorescent sensor enables rapid and specific detection of dopamine in flies, fish, and mice

Fangmiao Sun[1,2,*], Jianzhi Zeng[1,2,3,*], Miao Jing[1,2,3,*], Jingheng Zhou[4], Jiesi Feng[1,2,3], Scott F. Owen[5], Yichen Luo[1], Funing Li[6], Takashi Yamaguchi[7], Zihao Yong[8], Yijing Gao[7], Wanling Peng[9,10], Lizhao Wang[11], Siyu Zhang[11], Jiulin Du[6,12], Dayu Lin[7,13,14], Min Xu[9,10], Anatol C. Kreitzer[5,15], Guohong Cui[4], Yulong Li[1,2,3]

[1]State Key Laboratory of Membrane Biology, Peking University School of Life Sciences, Beijing 100871, China

[2]PKU-IDG/McGovern Institute for Brain Research, Beijing 100871, China

[3]Peking-Tsinghua Center for Life Sciences, Beijing 100871, China

[4]Laboratory of Integrative Neuroscience, National Institute on Alcohol Abuse and Alcoholism, National Institutes of Health, Rockville, MD, USA

[5]Gladstone Institutes, San Francisco, CA 94158, USA

[6]Institute of Neuroscience, State Key Laboratory of Neuroscience, CAS Center for Excellence in Brain Science and Intelligence Technology, Shanghai Institutes for Biological Sciences, Chinese Academy of Sciences, Shanghai, China

[7]Neuroscience Institute, New York University School of Medicine, New York, NY, USA

[8]College of Biological Sciences, China Agricultural University, Beijing 100193, China

[9]Chinese Academy of Sciences Center for Excellence in Brain Science and Intelligence Technology, Chinese Academy of Sciences, Shanghai 200031, China

[10]Institute of Neuroscience, Chinese Academy of Sciences, Shanghai 200031, China

[11]Shanghai Jiao Tong University School of Medicine, Shanghai 200025, China

[12]University of Chinese Academy of Sciences, Beijing, China

[13]Department of Psychiatry, New York University School of Medicine, New York, NY, USA

[14]Center for Neural Science, New York University, New York, NY, USA

[15]Gladstone Institutes, San Francisco, CA, USA; Department of Neurology, UCSF, San Francisco, CA, USA; Kavli Institute for Fundamental Neuroscience, UCSF, San Francisco, CA, USA; UCSF Weill Institute for Neurosciences, UCSF, San Francisco, CA, USA; Department of Physiology, UCSF, San Francisco, CA 94158, USA

*These authors contributed equally to this work

Manuscript correspondence:

Yulong Li (yulongli@pku.edu.cn)

Abstract

Dopamine (DA) is a central monoamine neurotransmitter involved in many physiological and pathological processes. A longstanding yet largely unmet goal is to measure DA changes reliably and specifically with high spatiotemporal precision, particularly in animals executing complex behaviors. Here we report the development of novel genetically-encoded GPCR-Activation-Based-DA ($GRAB_{DA}$) sensors that enable these measurements. In response to extracellular DA rises, $GRAB_{DA}$ sensors exhibit large fluorescence increases ($\Delta F/F_0$~90%) with sub-second kinetics, nanomolar to sub-micromolar affinities, and excellent molecular specificity. Importantly, $GRAB_{DA}$ sensors can resolve a single-electrical-stimulus evoked DA release in mouse brain slices, and detect endogenous DA release in the intact brains of flies, fish, and mice. In freely-behaving mice, $GRAB_{DA}$ sensors readily report optogenetically-elicited nigrostriatal DA release and depict dynamic mesoaccumbens DA changes during Pavlovian conditioning or during sexual behaviors. Thus, $GRAB_{DA}$ sensors enable spatiotemporal precise measurements of DA dynamics in a variety of model organisms while exhibiting complex behaviors.

Introduction

Dopamine is a crucial monoamine neurotransmitter in both vertebrates and invertebrates. In the vertebrate central nervous system, DA regulates a wide range of complex processes, including reward signaling (Schultz, 2016; Wise, 2004), reinforcement learning (Holroyd and Coles, 2002), attention (Nieoullon, 2002), motor control (Graybiel et al., 1994), arousal (Kume et al., 2005; Wisor et al., 2001), and stress (Abercrombie et al., 1989). In the human brain, impaired DA transmission is associated with neuropsychiatric disorders and neurodegenerative diseases, including attention deficit hyperactivity disorder (Cook Jr et al., 1995), schizophrenia (Howes and Kapur, 2009) and Parkinson's disease (Lotharius and Brundin, 2002). Moreover, psychostimulants, such as cocaine and amphetamine, exert their addictive effects by targeting components in the DA signaling pathway and by altering extracellular DA levels (Di Chiara and Imperato, 1988; Giros et al., 1996; Hernandez and Hoebel, 1988; Ritz et al., 1987).

Despite many important roles that DA plays in both physiological and pathological processes, precise measurements of the spatial and temporal patterns of DA release during complex behaviors are lacking. This gap in understanding due in large part to the limitation associated with existing methods for the real-time detection of endogenous DA release in the intact brain. Historically, intracerebral microdialysis has served as the gold standard for quantitative measurements of extracellular DA concentration. However, the relative slow sampling rate afforded by microdialysis is not well suited to detect dynamic changes in DA levels during complex and rapidly evolving behaviors, such as those that characterize social affiliation (Tidey and Miczek, 1996), aggression (van Erp and Miczek, 2000), and mating (Pfaus et al., 1990a, b). Fast-scan cyclic voltammetry (FSCV) is a temperamental electrochemical method that can measure changes in extracellular DA concentrations with 10-ms temporal resolution (Robinson et al., 2008; Rodeberg et al., 2017). However, because FSCV requires oxidization of DA molecules, it is difficult to distinguish DA from other structurally similar transmitters, such as norepinephrine (NE) (Robinson et al., 2003). Moreover, both microdialysis and FSCV require implantation of a relatively large probe or electrode (approximately 70-300 μm in diameter) into a specific brain region, which precludes the ability to obtain spatially precise measurements of endogenous DA release (Jaquins-Gerstl and Michael, 2015).

In lieu of direct measurements of extracellular DA, indirect methods, for example, measuring the activity of dopaminergic neurons (DANs) or the activation of DA receptor downstream targets, have also been used to approximate the dynamics of DA release. Genetic expression of a presynaptic tethered Ca^{2+} indicator in DANs has been used to indicate potential compartmentalized DA signals in the *Drosophila* olfactory pathway (Cohn et al., 2015). However, given the highly complex regulation of presynaptic Ca^{2+}, the nonlinear relationship between intracellular Ca^{2+} and transmitter release, as well as the active uptake of extracellular DA by transporters, it is difficult to quantitatively translate Ca^{2+} signals precisely into extracellular DA levels. Cell-based DA reporters, such as CNiFERs (Muller et al., 2014), use transplated HEK293 cells constitutively expressing DA receptors together with an intracellular Ca^{2+} indicator to couple extracellular DA signals with the fluorescence increase. However, This approach requires cell transplantation, which may limit the broad usage of this method. Moreover, CNiFERs are not spatially sensitive to synaptically released DA and thus may be limited to measurements of volumetric transmission of DA. Finally, the TANGO assay and their next-generation versions (Barnea et al., 2008; Inagaki et al., 2012; Kim et al., 2017; Lee et al., 2017) have been used to measure endogenous DA release by coupling the β-arrestin signaling pathway to reporter gene expression. Although this approach enables the cell-type specific expression of the DA reporter and is suitable for *in vivo* measurements, the long signal amplification time (on the order of hours) required for this assay precludes the ability to monitor rapid, physiologically relevant dynamics of DA signaling in real time.

Here, we report the development of novel, genetically-encoded sensors that enable direct, rapid, sensitive, and cell-type specific detection of extracellular DA. These sensors, which we call $GRAB_{DA}$ sensors, were engineered by coupling a conformationally sensitive circular-permutated EGFP (cpEGFP) to a selected human DA receptor. Through iterative engineering and optimization, we yielded two $GRAB_{DA}$ sensors: $GRAB_{DA1m}$, with medium DA affinity (EC_{50} ~ 130 nM); and $GRAB_{DA1h}$, with high DA affinity (EC_{50} ~ 10 nM). We show that these two newly developed $GRAB_{DA}$ sensors enable real-time detection of endogenous DA in acute brain slices of mice and in the intact brains of versatile animal models including flies, fish, and mice.

Results

Development and initial characterization of $GRAB_{DA}$ sensors

To develop a genetically encoded sensor for DA, we sought to engineer naturally evolved DA receptors to couple a conformationally sensitive cpEGFP. We hypothesized that upon DA binding, the conformational changes in the receptor could alter the arrangement of the associated cpEGFP, resulting in a DA-dependent change in fluorescence. Indeed, a similar strategy was recently applied in creating the genetically encoded acetylcholine sensor GACh (Miao Jing et al., 2018), suggesting that this strategy could potentially be expanded to generate DA sensors.

We used a three-step approach to engineer and optimize $GRAB_{DA}$ sensors (Fig. 1A-C): First, as the third intracellular loop (ICL3) of the G protein-coupled receptor (GPCR) links transmembrane V and VI that are thought to undergo large conformational changes upon ligand binding (Kruse et al., 2013), a cpEGFP was first inserted into the ICL3 of all five subtypes of human dopamine receptors (DRs); we subsequently focused on the D_2R-cpEGFP chimera due to its superior membrane trafficking and relatively high affinity for DA (Beaulieu and Gainetdinov, 2011; Missale et al., 1998) (Fig. S1A,B). In the second step, the position of the cpEGFP insertion within the ICL3, and individual amino-acids in the linker region between cpEGFP and D_2R were systematically screened (Fig. 1A,B). Finally, mutations at residues critical for receptors affinity for DA (Sung et al., 2016) were further introduced to expand the sensor's response range (Fig. 1C). After screening a total of more than 432 variants, we chose two, $GRAB_{DA1m}$ and $GRAB_{DA1h}$, both of which have a ~90% maximal $\Delta F/F_0$ response to the application of saturating levels of DA (Fig. 1B,E), but differ by an order of magnitude with respect to affinity for DA (130 nM for $GRAB_{DA1m}$ and 10 nM for $GRAB_{DA1h}$) (Fig. 1C). We also generated a corresponding mutant variant of each sensor ($GRAB_{DA1m\text{-}mut}$ and $GRAB_{DA1h\text{-}mut}$) by introducing C118A and S193N double mutations in the receptor's putative DA-binding pocket in order to abolish the DA binding (Chien et al., 2010b; Wang et al., 2018) (Fig. S1D). These so-called "dead" mutants exhibited no DA-induced change in fluorescence compared with $GRAB_{DA1m}$ and $GRAB_{DA1h}$ (Fig. 1D).

We next characterized the properties of the two $GRAB_{DA}$ sensors in detail in

cultured HEK293T cells. Both $GRAB_{DA1m}$ and $GRAB_{DA1h}$ trafficked efficiently to the plasma membrane of HEK293T cells (Fig. 1D and Fig. S1C). Cells expressing $GRAB_{DA1m}$ and $GRAB_{DA1h}$ exhibited robust fluorescence increases upon bath application of DA (Fig. 1D-F). Notably, the DA-induced fluorescence increase was completely blocked by the co-application of the D_2R antagonist haloperidol (Halo) (Sokoloff et al., 1990), confirming the molecular specificity of these sensors (Fig. 1E). Both mutant forms of $GRAB_{DA}$ sensors trafficked normally to the plasma membrane, similar to $GRAB_{DA1m}$ and $GRAB_{DA1h}$ (Fig. 1D and Fig. S1C), albeit with no detectable fluorescence increase in response to DA application (Fig. 1D,E). To characterize the response kinetics of $GRAB_{DA1m}$ and $GRAB_{DA1h}$, agonists or antagonists at high concentrations were locally applied to HEK293T cells expressing these sensors via a rapid perfusion system (Fig. 1F,G). Both $GRAB_{DA1m}$ and $GRAB_{DA1h}$ showed rapid fluorescence increases (on rate) in response to DA application, with a time constant of ~100 ms (60 ± 10 ms for $GRAB_{DA1m}$ and 140 ± 20 ms for $GRAB_{DA1h}$, respectively), implying that $GRAB_{DA}$ sensors are suitable for tracking rapid DA dynamics. The fluorescence decrease (off rate) of the $GRAB_{DA}$ sensors in response to applications of the antagonist Halo is slower in $GRAB_{DA1h}$ (2.5 ± 0.3 s) compared with $GRAB_{DA1m}$ (0.7 ± 0.06 s), consistent with the differences in affinity (Fig. 1G). We also measured the photostability of $GRAB_{DA1m}$ and $GRAB_{DA1h}$ in HEK293T cells. Under confocal laser illumination, both $GRAB_{DA}$ sensors were significantly more photostable than a membrane targeted EGFP or the glutamate sensor iGluSnFR (Marvin et al., 2013) (Fig. S2), suggesting that these new DA sensors are suitable for long-term measurements of DA dynamics.

We also tested the specificity of $GRAB_{DA}$ sensors for DA comparing with other neurotransmitters. HEK293T cells expressing $GRAB_{DA}$ sensors were sequentially perfused with solutions containing different neurotransmitters (Fig. 1H and Fig. S3; all were applied at 1 μM concentration). Again, bath application of DA induced robust fluorescence increases in both $GRAB_{DA1m}$- and $GRAB_{DA1h}$-expressing cells, and these signals were completely blocked by co-application of D_2R antagonists Halo or eticlopride (Etic), but not by the D_1R antagonist SCH-23390 (SCH). In contrast, applications of various other neurotransmitters, including serotonin (5-HT), histamine (His), glutamate (Glu), GABA, adenosine (Ade), acetylcholine (ACh), tyramine (Tyr), octopamine (Oct), glycine (Gly), or the DA precursor L-DOPA, did not elicit any detectable fluorescence changes (Fig. 1H and Fig. S3). We found that NE application evoked a small yet significant increase in fluorescence in both $GRAB_{DA1m}$- and $GRAB_{DA1h}$-expressing cells, although this increase was considerable smaller

than the response elicited by DA applied at the same concentration (for $GRAB_{DA1m}$, the $\Delta F/F_0$ in response to NE is 26% of that to DA). Further characterization of the affinity of $GRAB_{DA1m}$ or $GRAB_{DA1h}$ to both DA and NE revealed a 10-fold higher affinity to DA against NE (Fig. 1H and Fig. S3), as expected from the specificity of native human D_2R to DA and NE (Lanau et al., 1997b). Overall, $GRAB_{DA1m}$ and $GRAB_{DA1h}$ sensors show rapid and highly sensitive responses to physiological ranges of DA with little or no sensitivity to almost all other neurotransmitters tested here.

Does ectopic expression of $GRAB_{DA}$ sensors elicit unintended signaling by coupling to GPCR's downstream pathways? To examine this, we separately tested the coupling efficacies of $GRAB_{DA}$ sensors to either G protein- or β-arrestin-dependent pathways that are known to be downstream of activated D_2R (Beaulieu and Gainetdinov, 2011). It is well established that the coupling of a G protein with its cognate GPCR significantly increases the receptor's binding affinity for its ligand (Kruse et al., 2013). We therefore used pertussis toxin (PTX), which potently and selectively blocks the coupling between Gi proteins and GPCRs, such as D_2R (Burns, 1988). In cells expressing either $GRAB_{DA1m}$ or $GRAB_{DA1h}$, co-expression of PTX did not significantly alter the sensors' affinity for DA, indicating that $GRAB_{DA}$ sensors do not couple extensively to Gi proteins (Fig. 1I). On the other hand, if the DA-binding of $GRAB_{DA}$ sensors activates the β-arrestin-dependent pathway, the resulting internalization of sensors would reduce the fluorescence at the plasma membrane of HEK293T cells (Luttrell and Lefkowitz, 2002). However, we observed stable membrane fluorescence of the $GRAB_{DA}$ sensor-expressing cells throughout a 2-hour exposure to DA at a saturation concentration (100 μM), suggesting no detectable activation of β-arrestin-dependent signaling under these conditions (Fig. 1J). Collectively, these data suggest that $GRAB_{DA}$ sensors do not engage these major downstream GPCR-mediated signaling pathways.

Characterization of $GRAB_{DA}$ in cultured neurons

We next evaluated the expression pattern and functional properties of $GRAB_{DA}$ sensors in cultured rat cortical neurons. After 48h expression, both $GRAB_{DA1m}$ and $GRAB_{DA1h}$ showed basal fluorescence signals in transfected neurons, with the brightest signal in the plasma membrane of somas and neurites, indicated by the colocalization with a membrane marker RFP-CAAX (Hancock et al.,

1991) (Fig. 2A,B and Fig. S4). In addition, co-expression of the $GRAB_{DA}$ sensors with the postsynaptic (PSD95-RFP) or presynaptic (SYP-RFP) markers revealed that $GRAB_{DA}$ sensors were distributed throughout the entire membrane in dendritic shafts, spines, axons and axonal boutons, suggesting the suitability of $GRAB_{DA}$ sensors to detect DA dynamics in sub-neuronal compartments (Fig. 2B and Fig. S4). As in HEK293T cells, DA application in transfected cultured neurons induced dose-dependent fluorescence increases in both $GRAB_{DA1m}$- and $GRAB_{DA1h}$-expressing neurons with a similar maximum $\Delta F/F_0$ of ~90%, and with an EC_{50} of ~170 nM and ~8 nM for $GRAB_{DA1m}$ and $GRAB_{DA1h}$, respectively (Fig. 2C-E). Moreover, the specificity of both $GRAB_{DA}$ sensors for DA was similar in cultured neurons compared to HEK 293T cells (Fig. 2F). Finally, no detectable decrease of surface fluorescence signals of $GRAB_{DA}$ sensors-expressing cells was observed in response to a 2-h continuous application of DA at a saturation concentration (100 μM) (Fig. 2G), suggesting that $GRAB_{DA}$ sensors were not internalized over this time frame. Collectively, these data demonstrate that $GRAB_{DA}$ sensors can monitor DA signals with high sensitivity and specificity in cultured rat cortical neurons.

Characterization of $GRAB_{DA}$ in acute brain slices

A crucial issue is whether $GRAB_{DA}$ sensors are sufficiently sensitive to detect and monitor endogenous DA release in native brain tissue. To begin to resolve this issue, we injected AAVs carrying either $GRAB_{DA1m}$ or $GRAB_{DA1h}$ into the nucleus accumbens (NAc) of mice, then prepared acute brain slices containing NAc two weeks later. Post hoc visualization in fixed brain slices revealed that the fluorescent signal of $GRAB_{DA}$ sensors could be detected in the NAc region of virus-injected mice, and the signal was in close proximity to putative DA-releasing fibers that were immunoreactive for tyrosine hydroxylase (TH) (Fig. 3A). Electrical stimulation within NAc core elicited robust and time-locked fluorescence increases in both $GRAB_{DA1m}$- and $GRAB_{DA1h}$-expressing neurons (Fig. 3A-C). Increasing the number of stimulation pulses or stimulation frequency resulted in a progressive increase in the intensity of evoked fluorescence signals in neurons expressing $GRAB_{DA1m}$ or $GRAB_{DA1h}$ (Fig. 3B,C). These stimulus-evoked fluorescent signals reached plateau levels at high stimulation frequency with large stimulation number (e.g. more than 50 pulses) in $GRAB_{DA1h}$ expressing neurons , presumably due to saturation of the sensor arising from $GRAB_{DA1h}$'s high affinity for DA. The rise times of stimulus-evoked fluorescence signals were fast in both $GRAB_{DA1m}$- and $GRAB_{DA1h}$-expressing neurons (Fig. 3D), whereas the decay time of fluorescent signals in $GRAB_{DA1h}$

expressing neurons was slower than that in neurons expressing GRAB$_{DA1m}$ (Fig. 3D), consistent with the DA affinity and response kinetics measured in cultured cells (see Fig. 1C,G). Repeated electrical stimuli delivered at 5-minute intervals evoked reproducible fluorescence responses, indicating the reliability and stability of GRAB$_{DA1m}$ and GRAB$_{DA1h}$ in reporting multiple DA releasing events (Fig. 3E). Bath application of the D_2R antagonist Halo abolished the electrically stimuli-induced fluorescence responses in either GRAB$_{DA1m}$- or GRAB$_{DA1h}$-expressing neurons (Fig. 3F), verifying the sensor's specificity when expressed in brain slices. Collectively, both GRAB$_{DA1m}$ and GRAB$_{DA1h}$ enable sensitive and specific detection of endogenous DA dynamics in acute mouse brain slices.

Imaging DA dynamics in *Drosophila*

We next examined the ability of GRAB$_{DA}$ sensors to detect physiologically relevant DA dynamics in living animals. We selected the fly as an initial test of our sensors, as DA plays a key role in the fly brain, serving as a critical teaching signal in olfactory-associative learning (Burke et al., 2012; Heisenberg, 2003; Liu et al., 2012; Schwaerzel et al., 2003). Transgenic UAS-GRAB$_{DA1m}$ flies were generated and first crossed with TH-GAL4 to express GRAB$_{DA1m}$ specifically in DANs. Two-photon imaging methods were used to study odor-evoked DA signals in the mushroom body (MB) in living flies (Fig. 4A). We found that the odorant isoamyl acetate (IA) elicited a time-locked fluorescence increase in the MB, most prominently in the β' lobes, and this IA-evoked response was blocked by Halo application. In contrast, no IA-evoked fluorescence response was observed in flies expressing GRAB$_{DA1m\text{-}mut}$ (Fig. 4B). To further test the signal specificity, we use the C305a-GAL4 line to express GRAB$_{DA1m}$ in Kenyon cells which receives direct input from DANs (Aso et al., 2010). Comparing wild-type (WT) control flies and TH-deficient flies (Cichewicz et al., 2017), which lack DA synthesis in the CNS. Compared with WT flies, we observed no detectable IA-evoked GRAB$_{DA1m}$ fluorescence increase was observed in TH-deficient flies (Fig. 4B,C). We also examined whether the ectopic expression of GRAB$_{DA}$ sensors may alter physiological properties, such as the neuronal excitability. We observed no significant difference between GRAB$_{DA}$ sensors-expressing and non-expressing DANs or Kenyon cells with respect to odor-evoked Ca^{2+} signals (Fig. S5), suggesting that expression of the sensor does not alter odor-evoked responses in neurons in the fly brain.

To further characterize the sensitivity and kinetics of GRAB$_{DA1m}$ *in vivo*, we

electrically stimulated MB DANs while simultaneously monitoring the corresponding fluorescence signals (Fig. 4D,E). We found that $GRAB_{DA1m}$-expressing DANs exhibited a reproducible fluorescence increases in response to repeated trains of electrical stimuli delivered at various frequencies, and even a single stimulus was sufficient to elicit a measurable increase in fluorescence (Fig. 4D,E). In contrast, similar electrical stimulation did not evoke any detectable fluorescence increase in flies expressing $GRAB_{DA1m\text{-}mut}$ (Fig. 4D,E). With the increase of pulse number delivered at 20 Hz, fluorescence signals of $GRAB_{DA1m}$ increased progressively and reached a plateau of peak $\Delta F/F_0$ of ~35% after 10 pulses (Fig. 4F-H). The fluorescence responses evoked by electrical stimulation exhibited sub-second kinetics, with on and off time constants of 0.07 ± 0.01 s and 0.39 ± 0.05 s, respectively (Fig. 4I), indicating the suitability of $GRAB_{DA1m}$ for monitoring endogenous transient DA signals. Consistent with the odor-evoked fluorescence increase, application of Halo completely blocked the fluorescence increases elicited by electrical stimuli (Fig. 4J,K), confirming the sensor's specificity.

The DA transporter (DAT), which is a highly conserved protein across insects and vertebrates, is responsible for the reuptake of DA from extracellular space for subsequent reuse, and is the primary target of many drugs of abuse (Bainton et al., 2000; Ritz et al., 1987). Impairing DAT function results in sustained elevation of extracellular DA levels (Fig. 4L) (Bainton et al., 2000; Ritz et al., 1987). To determine whether our sensor could detect changes in extracellular DA arising from manipulation of the DAT, we applied cocaine, a psychostimulant drug that blocks DAT. Cocaine significantly potentiated the odor-evoked fluorescence increase of $GRAB_{DA1m}$ expressed in MB DANs, and this cocaine-potentiated response was accompanied by a prolonged decay in the fluorescence signal (Fig. 4M-O). Genetically knocking down the expression of DAT selectively in DANs phenocopied the effect of cocaine administration (Fig. 4M-O), confirming the ability of $GRAB_{DA1m}$ to measure the dynamic regulation of DA release and reuptake *in vivo*. Together with our results described above, these data demonstrated that $GRAB_{DA}$ sensors have the sensitivity, fast kinetics, and specificity to report *in vivo* DA dynamics in genetically-defined neurons in the intact brain of living flies.

Imaging DA release in the intact zebrafish brain

Zebrafish larvae have an optically transparent brain and is capable of

performing a wide range of behaviors, affording a powerful system to explore the structure and function of the vertebrate brain at cellular resolution in a behavioral framework. To test the feasibility of using $GRAB_{DA}$ sensors in imaging DA dynamics in zebrafish larvae, we generated the transgenic line Tg(elval3:$GRAB_{DA1m}$/DAT:TRPV1-TagRFP), in which $GRAB_{DA1m}$ was expressed pan-neuronally throughout the brain, and TRPV1-TagRFP was expressed specifically in DANs to enable their chemogenetic activation by capsaicin (Fig. 5A). We first applied DA to the fish, and observed fluorescence increases in $GRAB_{DA1m}$-expressing neurons in the head, which were blocked by co-application of antagonist Halo, suggesting the specificity of $GRAB_{DA}$ (Fig. 5B-D).

Next, we hope to track the dynamics of endogenous DA signals in zebrafish larvae. We previously reported that the optic tectum of zebrafish larvae receives synaptic input from pretectal DANs (Shang et al., 2015), advancing the tectum as a potential site to monitor DA release. We therefore performed confocal imaging of $GRAB_{DA1m}$-expressing tectal neurons in the live transgenic zebrafish larvae (Fig. 5E). Repeated application of capsaicin (five 100-ms puffs delivered with a 1-min interval) caused the progressive increase in the fluorescence signals in the tectal neuropil (Fig. 5F-H). The capsaicin-induced fluorescence increase was again abolished by the application of Halo (Fig. 5F-H), confirming that the response was specifically due to $GRAB_{DA1m}$ activation. Thus, the $GRAB_{DA1m}$ is well suited to report *in vivo* DA dynamics in the brain of zebrafish larvae.

Combining optogenetics with $GRAB_{DA}$ to measure the dynamics of DA in freely moving mice

To test the ability of $GRAB_{DA}$ sensors to report DA dynamics in specific circuits in the mouse brain *in vivo*, we focused on DANs located in the substantia nigra pars compacta (SNc) that project to the dorsal striatum (Str). This nigrostriatal pathway is implicated in complex behavioural functions including motivation, reward, and learning (Balleine et al., 2007; Da Silva et al., 2018; Howe and Dombeck, 2016). We virally expressed DIO-C1V1 (Yizhar et al., 2011) in the SNc of TH-Cre mice, permitting selective optogenetic activation of DANs. Additionally, we virally co-expressed $GRAB_{DA1m}$ and tdTomato in the dorsal striatum, allowing us to simultaneously monitor DA release using the green ($GRAB_{DA1m}$) channel while detecting movement-related fluorescence artefacts

using the red (tdTomato) channel (Fig. 6A,B, see methods for detail). In free moving mice, the ratio of $GRAB_{DA1m}$ to tdTomato fluorescence was elevated upon the administration of methylphenidate, a known DAT blocker (Volkow et al., 1999) (Fig. 6C, top), and was suppressed by subsequent administration of Etic (Fig. 6C, top), a D_2R blocker, implying the ability of $GRAB_{DA}$ sensors in reporting DA dynamics to pharmacological treatments. Interestingly, we observed fluctuations in the ratio of $GRAB_{DA1m}$ to tdTomato fluorescence that likely reflect the spontaneous DA release during the animal movements (Balleine et al., 2007; Da Silva et al., 2018; Howe and Dombeck, 2016), as they were prolonged during methylphenidate application and largely diminished by Etic administration (Fig. 6C, bottom).

Combining optogenetic stimulation and fiber photometry in freely moving mice, we observed that C1V1-evoked activation of DANs in the SNc generated a time-locked transient fluorescence increase in the dorsal striatum specific to the $GRAB_{DA1m}$ channel (Fig. 6D), consistent with the evoked DA release from SNc DAN terminals. Systemic administration of the DA transporter blocker methylphenidate significantly prolonged the decay of optogenetically-evoked $GRAB_{DA1m}$ fluorescence responses in the dorsal striatum (Fig. 6D,E). Furthermore, administration of D_2R antagonist Etic largely abolished the response (Fig. 6D,F). Therefore, the $GRAB_{DA}$- and C1V1- based all-optical approach is effective for monitoring spontaneous and optogenetically-evoked DA release in the nigrostriatal pathway of mice.

Bi-directional modulation of DA dynamics in the nucleus accumbens (NAc) during Pavlovian conditioning

In addition to the nigrostriatal pathway, the dopaminergic projection from the ventral tegmental area (VTA) to the nucleus accumbens (NAc) regulates a variety of important functions including the reinforcement learning (Daw and Tobler, 2013; Glimcher, 2011; Gonzales et al., 2004), wherein an animal learns to associate an initially neutral sensory cue, such as a short tone burst, with an ensuing reward or punishment. Previous studies show that DANs in the VTA fire phasically to unpredicted rewards or reward-predicting cues and, with conditioning, the reward-evoked response diminishes as it becomes fully predicted by the cue (Bayer and Glimcher, 2005; Schultz, 2006; Schultz et al., 1997). To test whether our sensor can detect behaviourally relevant changes in endogenous DA release, we first expressed $GRAB_{DA1h}$ in the NAc of head-fixed,

water-restricted mice and trained them to associate a brief auditory cue with subsequent delivery of a liquid sucrose water reward (Fig. 7A). Each mouse experienced two distinct auditory cues, one that predicted delivery of a reward within a variable delay of 500-1500 ms after the end of the cue, as well as a second, randomly interleaved control cue (No Water, N.W.) that was not associated with water reward. Mice were trained daily for ~10 days, and the $GRAB_{DA1h}$ signal was recorded using *in vivo* fiber photometry in both the early and late stages of training. Consistent with the expected DA signaling in this classical paradigm, elevations in the $GRAB_{DA1h}$ fluorescent signal aligned to reward delivery in every mouse, immediately in the first session without requiring training (Fig. 7C,E). After 6-10 days of training, mice selectively learned to associate the reward-predictive cue with delivery of reward. Consistent with the established reward prediction error theory of DA function, DA signals emerged in trained mice in response to the reward-predicting cue before the delivery of the reward (Fig. 7B,D-F). These results demonstrate that the signal-to-noise and temporal resolution of $GRAB_{DA1h}$ is sufficient to detect physiologically relevant DA signaling *in vivo* in awake, behaving mice. Furthermore, these results serve to validate the $GRAB_{DA1h}$ recorded DA signals by anchoring them to decades of established basal ganglia and the physiology of DA neurons.

In addition to transient elevations in DA signal in response to unexpected reward, DA neuron firing dips briefly in response to aversive stimuli (Brooks and Berns, 2013; Schultz, 2007; Ungless et al., 2004). We expressed the lower affinity $GRAB_{DA1m}$ in the NAc of mice and trained them to associate a tone burst with an ensuing reward (a drop of water), or a punishment (a brief air puff to the face) to test whether our sensor can detect bi-directional changes in DA tone. During training, mice learned the association between an auditory cue and several outcomes (Fig. 7A). *In vivo* fiber photometry recording of $GRAB_{DA}$ signals revealed that during early stages of training, reward or punishment delivery triggered a robust increase or decrease in the fluorescence signal in the NAc (Fig. 7G,H). Over the course of training, the magnitude of this reward-evoked response decreased, while a response of similar sign developed to the associated cue (Fig. 7G,H). In summary, the $GRAB_{DA}$ sensor can be used to report the dynamic bi-directional changes in DA release over the course of Pavlovian conditioning.

Monitoring DA release in the NAc of mice during male mating behaviors

In contrast to the well-established involvement of DA in Pavlovian conditioning, DA dynamics during naturally rewarding social behaviors (Berridge and Robinson, 1998), such as courtship and mating, remains largely a subject of debate. Microdialysis and voltammetric measurements have previously revealed a relatively slow change in DA concentration during sexual behaviors: DA levels in the male's NAc start to increase after a female is introduced into his cage and continues to rise throughout the course of sexual behaviors and ejaculation (~20 minutes), then slowly (~30 minutes) return to baseline after the female is removed (Damsma et al., 1992; Mas et al., 1995; Pfaus et al., 1990b). In contrast, a more recent study using FSCV showed that DA is transiently released in the male's NAc when the female is introduced but few changes in DA levels were detected during subsequent sexual behaviors (Robinson et al., 2002; Robinson et al., 2001). To better understand DA dynamics during sexual behaviors, we virally expressed $GRAB_{DA1h}$ in the NAc of male mice and used fiber photometry to record DA signals during sexual behaviors (Fig. 8A). Four weeks after injection, a sexually receptive C57BL/6 female was introduced into the home cage of the male mouse. Upon a female introduction, the male quickly approached and investigated the female, and then initiated mounting within the first minute. The $GRAB_{DA1h}$ signals measured in the male's NAc acutely and consistently increased with investigation of the female, mounting, intromission, ejaculation, and penile grooming (Fig. 8B). When we aligned the $GRAB_{DA1h}$ signals with the manually annotated behaviors for each male, we observed that fluorescence signals increased prior to the corresponding behavior, peaked at the behavior's onset, and then gradually declined (Fig. 8C). Among all of the sexual behaviors we annotated, the largest fluorescence increase occurred during intromission and ejaculation (Fig. 8C,D). These results indicate that DA in the NAc is acutely released during episodes of sexual behaviors and may carry information regarding specific features of courtship and/or mating.

Discussion

Here we describe the development and characterization of a pair of novel genetically-encoded sensors that enable specific, real-time detection of endogenous DA dynamics in various *ex vivo* and *in vivo* preparations and model systems. In acute mouse brain slices, $GRAB_{DA}$ sensors were well suited to monitor stimulus-evoked DA release in mesolimbic pathway. In flies, $GRAB_{DA}$ sensors were sufficiently sensitive to detect DA release in the MB triggered by odorants presented at physiologically relevant concentrations, and could also readily resolve DA release evoked by a single electrical stimulus. In transgenic zebrafish, $GRAB_{DA}$ sensors were able to report DA release in the optic tectum

in response to the chemogenetic activation of pretectal DANs. In mice, combining optogenetic stimulation with $GRAB_{DA}$ sensors enabled the simultaneous optical manipulation and detection of DA signals *in vivo*. Finally, $GRAB_{DA}$ sensors revealed real-time DA dynamics in the NAc of freely behaving mice as they underwent Pavlovian conditioning or engaged in sexual behaviors.

Compared to current methods used to measure DA release, our $GRAB_{DA}$ sensors described here exhibit several clear advantages. First, $GRAB_{DA}$ sensors are genetically-encoded by relatively small genes (~2 kb), making them highly amenable to transgenic approaches and viral packaging. Second, $GRAB_{DA}$ sensors have high sensitivity to DA. In response to DA, $GRAB_{DA1m}$ and $GRAB_{DA1h}$ sensors are capable of achieving maximal $\Delta F/F$ ~ 90% with ~10 nM and ~100 nM affinities, respectively. In contrast, conventional GPCR-based FRET probes for detecting neurotransmitters are usually limited to a maximum FRET signal changes of ~ 5% under optimal conditions, and less than that *in vivo* (Vilardaga et al., 2003; Ziegler et al., 2011). Third, $GRAB_{DA}$ sensors have high specificity to DA: A range of experimental approaches, including application of multiple neurotransmitters and D_2R antagonists, perturbation of DATs, or manipulation of DA synthesis pathways unequivocally support the molecular specificity of $GRAB_{DA}$ sensors for DA. Notably, similar to the human D_2R upon which they are based, both $GRAB_{DA}$ sensors have a 10-fold higher affinity for DA than for NE (Lanau et al., 1997b); in contrast, FSCV is unable to discriminate between these two catecholamines (Fox and Wightman, 2016; Park et al., 2009). Finally, $GRAB_{DA}$ sensors have extremely rapid response kinetics: $GRAB_{DA}$ sensors report increases in DA levels with a rise time of ≤ 100 ms (Fig. 1G, 3D and 4I). Although this response time of $GRAB_{DA}$ sensors is slower than voltammetry methods, it is still sufficiently rapid for reporting physiologically relevant DA dynamics and share response kinetics similar to WT GPCRs (Lohse et al., 2008), providing an accurate readout of their activation.

Because $GRAB_{DA}$ sensors were engineered using the D_2R, a G_i-coupled GPCR, a potential concern is that overexpressing the $GRAB_{DA}$ sensors may inadvertently activate pathways downstream of D_2R. However, several lines of evidence argue against this possibility, including the negligible coupling between $GRAB_{DA}$ sensors and both G protein-dependent and arrestin-dependent intracellular signaling pathways, alleviating this concern (Fig. 1I, 1J). This lack of coupling is presumably due to the steric hindrance imposed by the bulky cpEGFP moiety that replaces parts of the ICL3, which is the critical position for G protein or arrestin to interact with the GPCR (Luttrell and

Lefkowitz, 2002; Neves et al., 2002). Consistent with minimal coupling between $GRAB_{DA}$ sensors and downstream signaling pathways, *in vivo* Ca^{2+} imaging experiments using the Ca^{2+} sensor jRCaMP1a revealed no measurable alteration in Ca^{2+} signaling in neurons of transgenic flies that overexpressing $GRAB_{DA}$ sensors (see Fig. S5).

In flies, DA signaling is critical for olfactory learning (Burke et al., 2012; Heisenberg, 2003; Liu et al., 2012; Schwaerzel et al., 2003). Here show that $GRAB_{DA}$ sensors can be targeted to specific cells in the fly brain and used to probe odor-evoked DA dynamics in the MB of the living fly in real-time. It is reported that different types of DANs innervate different compartments of MBs, and these different dopaminergic pathways may play distinct roles in appetitive and aversive olfactory-dependent behaviors (Aso and Rubin, 2016; Cognigni et al., 2017). The $GRAB_{DA}$ sensors developed here create new opportunities for exploring how distinct DA dynamics can correspond with specific compartments in the MB of the intact fly, particularly as the animal engages in different behavioral paradigms. Experiments in flies also illustrate the power of $GRAB_{DA}$ sensors to probe DAT function *in vivo* by directly measuring extracellular DA level in real time. Similarly, we showed that $GRAB_{DA}$ sensors readily respond to DA transients in the intact brain of the zebrafish larvae, providing a robust and convenient tool to examine DA dynamics in this classic vertebrate model system.

In addition to the morphological distinctions that can be made between various DANs in the mammalian CNS, breakthroughs in single-cell sequencing have further divided these neurons into a wide variety of cell types with distinct molecular features, suggesting high functional heterogeneity (Nair-Roberts et al., 2008; Ungless and Grace, 2012). Therefore, genetically-encoded $GRAB_{DA}$ sensors provide a novel tool to explore patterns of DA release from genetically distinct DAN types, thereby facilitating the understanding of how they may be functionally specialized for different physiological and behavioral processes (Lammel et al., 2014; Pignatelli and Bonci, 2015). In fact, $GRAB_{DA}$ sensors applied in the mouse faithfully reported the expected bi-directional regulation of DA levels in the NAc during different forms of Pavlovian conditioning. Consistent with the notion that DA can predict an anticipated reward (Schultz et al., 1997), the $GRAB_{DA}$ sensor detected a robust, phasic increase in DA levels that shifted from reward onset to cue onset over the course of reward learning. Conversely, in naïve animals, a transient decrease in DA levels was triggered by the air puff onset and this decrease shifted to cue onset during

aversive conditioning. An important goal of future studies will be to use $GRAB_{DA}$ sensors to determine whether the same or different types of DANs are involved in appetitive vs. aversive learning.

Our experiments in freely behaving male mice provide new perspectives with respect to DA dynamics during sexual behaviors. Contrary to traditional views, $GRAB_{DA}$ sensors expressed in the NAc revealed striking time-locked DA elevation immediately prior to and peak at the onset of various distinct sexual behaviors, consistent with a model where DA encodes behavioral motivation, anticipation, or arousal. These rapid changes in DA levels are in contrast with previous dialysis studies showing that DA levels in the NAc slowly increase during sexual behaviors, a difference that likely relates to the slow readout associated with dialysis-based methods. The targeted expression of $GRAB_{DA}$ sensors could therefore provide a critical window into the coding strategy of DA release in complex behaviors. Moreover, because $GRAB_{DA}$ sensors readily discriminate between DA and NE, they may be useful in studying cortical and subcortical regions in which dopaminergic and adrenergic inputs are intertwined.

Given that the crystal structure of the D_2R was recently solved (Wang et al., 2018), future efforts can use this structural information to further tune the affinity, enhance the selectivity, and increase the signal-to-noise ratio in the next-generation of $GRAB_{DA}$ sensors. Moreover, by adding a red fluorescent protein, $GRAB_{DA}$ sensors can be readily transformed into ratiometric indicators, which could prove useful for more quantitative measurements of DA release across different experiments and preparations. Finally, a GPCR-based strategy was recently used to develop a genetically-encoded sensor (GACh) with high sensitivity and high selectivity for acetylcholine (ACh) (Miao Jing et al., 2018). Although the GACh sensor differs from the $GRAB_{DA}$ sensors described here in that is based on the muscarinic Gq-coupled GPCR receptor M_3R and an ICL3 loop derived from a Gs-coupled beta adrenergic receptor (Levitzki, 1988; Rasmussen et al., 2011), a feature common to this sensor is that the conformational changes in a GPCR induced by ligand binding are successfully harnessed and converted into a sizable increase in cpEGFP florescence. Given the diverse ligand-specificity of different GPCRs, a future goal will be to explore whether this principle can be expanded even further in order to develop sensors for the entire range of neurotransmitters and neuromodulators.

Methods

Animals

Wild-type Sprague-Dawley rat pups (P0) were used to prepare cultured cortical neurons. Wild-type C57BL/6 and TH-Cre mice (B6.FVB(Cg)-Tg(Th-cre)FI172Gsat/Mmucd obtained from MMRRC) were used to prepare the acute brain slices and *in vivo* experiments. All animals were maintained in the animal facilities and were family- or pair-housed in a temperature-controlled room with a 12-h/12-h light/dark cycle. All procedures for animal surgery and maintenance were performed using protocols that were approved by the Animal Care & Use Committees at Peking University, Chinese Academy of Sciences (CAS), New York University, University of California, San Francisco, and US National Institutes of Health, and were performed in accordance with the guidelines established by US National Institutes of Health guidelines.

To generate transgenic zebrafish, plasmids containing pTol2-elval3:GRAB$_{DA1m}$ (25 ng/μL) and Tol2 mRNA (25 ng/μL) were co-injected into fertilized eggs, and founders were screened three months later. Transgenic zebrafish adults and larvae were maintained at 28 °C on a 14-h/10-h light/dark cycle.

To generate transgenic flies, the coding sequence of GRAB$_{DA1m}$ was integrated into the pUAST vector using Gibson Assembly (Gibson et al., 2009), which was then used in P-element-mediated random insertion. Transgenic *Drosophila* lines carrying GRAB$_{DA1m}$ on the chromosomes 2 and 3 with the strongest expression level after crossing with TH-GAL4 were used. The coding sequence of GRAB$_{DA1m-mut}$ was incorporated into pJFRC28 (Pfeiffer et al., 2012) (Addgene plasmid #36431) using Gibson Assembly, and this plasmid was used to generate transgenic flies using PhiC31-mediated site-directed integration into attp40. The embryo injections were performed at Core Facility of Drosophila Resource and Technology, Shanghai Institute of Biochemistry and Cell Biology, CAS. Transgenic flies were raised on conventional corn meal at 25°C, with ~70% humidity, under 12:12-h light-dark cycle.

The following *Drosophila* lines used in this study:

TH-GAL4, a gift and unpublished line generated by appending 2A-GAL4 to the last exon of TH, from Yi Rao, Peking University. C305a-GAL4 and 30y-GAL4,

671 also gifts from Yi Rao. $DTH^{FS+/-}ple^{2}$/TM6B (Cichewicz et al., 2017), a gift from
672 Jay Hirsh, University of Virginia. UAS-DAT-RNAi (TH01470.N), from Tsinghua
673 Fly center, Tsinghua University. UAS-jRCaMP1a (Bloomington #63792), a gift
674 from Chuan Zhou, Institute of Zoology, Chinese Academy of Sciences.

675 The following genotypes were used in the following figures:

676 Fig. 4A-C

677 UAS-$GRAB_{DA1m}$/cyo; TH-GAL4 (DANs)/TM6B

678 UAS-$GRAB_{DA1m\text{-}mut}$/+; TH-GAL4/+

679 c305a-GAL4 (α' and β' Kenyon cells)/UAS-$GRAB_{DA1m}$; $DTH^{FS+/-}ple^{2}$/+ (WT
680 group)

681 c305a-GAL4/UAS-$GRAB_{DA1m}$; $DTH^{FS+/-}ple^{2}$ (TH-deficient group)

682 Fig. 4D-K

683 UAS-$GRAB_{DA1m}$/cyo; TH-GAL4/TM6B

684 UAS-$GRAB_{DA1m\text{-}mut}$/+; TH-GAL4/+

685 Fig. 4L-O

686 UAS-$GRAB_{DA1m}$/cyo; TH-GAL4/TM6B

687 UAS-$GRAB_{DA1m}$/+; TH-GAL4/UAS-DAT-RNAi

688 Fig. S5

689 TH-GAL4/ UAS-jRCaMP1a

690 UAS-$GRAB_{DA1m}$/+; TH-GAL4/UAS-jRCaMP1a

691 30y-GAL4/ UAS-jRCaMP1a

692 UAS-$GRAB_{DA1m}$/+; 30y-GAL4/UAS-jRCaMP1a

693

694 **Molecular biology**

695

696 Plasmids were generated using Gibson Assembly. DNA fragments were
697 generated using PCR amplification with primers (Thermo Fisher Scientific) with
698 30-bp overlap. The fragments were assembled using T5-exonuclease (New
699 England Biolabs), Phusion DNA polymerase (Thermo Fisher Scientific), and
700 Taq ligase (iCloning). All sequences were verified using Sanger sequencing
701 (Sequencing platform in the School of Life Sciences of Peking University). DNA

encoding the various DA receptor subtypes (D_1R-D_5R) was generated using PCR amplification of the full-length human GPCR cDNAs (hORFeome database 8.1). For characterization in HEK293T cells, the $GRAB_{DA}$ constructs were cloned into the pDisplay vector (Invitrogen), with an IgK leader sequence inserted upstream of the coding region. The IRES-mCherry gene was attached downstream of $GRAB_{DA}$ and was used as a reference of membrane marker to calibrate of the signal intensity. Site-directed mutagenesis of the N- and C-terminal linker sequences in cpEGFP was performed using primers containing randomized NNB codons (48 codons in total, encoding the 20 possible amino acids; Thermo Fisher Scientific). Site-directed mutagenesis of the D_2R gene was performed using primers containing the target sites. For the characterization in cultured neurons, the $GRAB_{DA}$ constructs were cloned into the pAAV vector under the TRE promoter or the human synapsin promoter. The marker constructs RFP(mScarlet)-CAAX, EGFP-CAAX, KDELR1-EGFP, PSD95-mScarlet and synaptophysin-mScarlet were cloned into pEGFP-N3 vector.

Expression of $GRAB_{DA}$ in cultured cells and *in vivo*

HEK293T cells were cultured in DMEM supplemented with 10% (v/v) FBS (Gibco) and 1% penicillin-streptomycin (Gibco) at 37°C in 5% CO_2. The cells were plated on 12-mm glass coverslips in 24-well plates and grown to ~50% confluence for transfection. Transfection was performed by incubating the HEK293T cells with a mixture containing 1 μg of DNA and 3 μg of PEI for 6 h. Imaging was performed 24-48 h after transfection.

Rat cortical neurons were prepared from postnatal 0-day old (P0) Sprague-Dawley rat pups as previously described (Zhang et al., 2009). In brief, the cortical neurons were dissociated from the dissected rat brains in 0.25% Trypsin-EDTA (Gibco), and plated on 12-mm glass coverslips coated with poly-D-lysine (Sigma-Aldrich) in neurobasal medium containing 2% B-27 supplement, 1% GlutaMax, and 1% penicillin-streptomycin (Gibco). The cells were transfected 7-9 days later using the calcium phosphate transfection method. Imaging was performed 48-72 h after transfection.

For *in vivo* expression, Wild-type C57/BL6 mice with the age of P42-60 were first anesthetized by 2,2,2-Tribromoethanol (Avetin, 500 mg/kg) through

intraperitoneal injection, or by isoflurane (RWD Life Science), and then placed in a stereotaxic frame to inject AAVs of $GRAB_{DA}$ sensors into NAc with a microsyringe pump (Nanoliter 2000 Injector, WPI), or a microinjection pipette injector (Nanoject II, Drummond Scientific). The coordination of NAc was set as AP: -1.40 mm from Bregma, ML: 1.00 mm from the midline, DV: 3.90 mm from the brain surface. The injection was made unilateral with ~300-500 nL per animal. In dual-color optical recordings experiments, the AAVs of hsyn-$GRAB_{DA1m}$ and hsyn-tdTomato were injected in the dorsal striatum (AP = -0.5mm, ML = ±2.5mm from bregma, and DV = -2.2mm from the brain surface), and AAV of Ef1a-DIO-C1V1-YFP was injected in the substantia nigra pars compacta (SNc) (AP = -3.1mm, ML = ±1.5mm from bregma, and DV = -4.0mm from the brain surface) in TH-Cre mice.

Fluorescence imaging of HEK293T cells and cultured neurons

$GRAB_{DA}$-expressing HEK293T cells and cultured neurons were imaged using an inverted Ti-E A1 confocal microscope (Nikon) and the Opera Phenix high content screening system (PerkinElmer). The Nikon confocal microscope was equipped with a 40×/1.35 NA oil immersion objective, a 488-nm laser and a 561-nm laser. During imaging, the HEK293T cells and cultured neurons were bathed or perfused in a chamber with Tyrode's solution containing (in mM): 150 NaCl, 4 KCl, 2 $MgCl_2$, 2 $CaCl_2$, 10 HEPES and 10 glucose (pH 7.4). Solutions containing the drug/compound of interest (e.g., DA, Halo, 5-HT, histamine, NE, or ACh) were delivered via a custom-made perfusion system or via bath application. The chamber was fully cleaned with Tyrode's solution and 75% ethanol between experiments. The GFP signals (e.g., the $GRAB_{DA}$ sensors, the iGluSnFR or EGFP) were recorded using a 525/50 nm emission filter, and the RFP signals were collected using a 595/50 nm emission filter. The photostabilities of $GRAB_{DA1m}$, $GRAB_{DA1h}$, EGFP, and iGluSnFR were measured using 350-μW 488-nm laser illumination. Photobleaching was applied to the entire sensor-expressing HEK293T cell. The Opera Phenix high content screening system was equipped with a 60×/ 1.15 NA water immersion objective, a 488-nm laser, and a 561-m laser. The $GRAB_{DA}$ signals were collected using a 525/50 nm emission filter, and the mCherry signals were collected using a 600/30 nm emission filter. Where indicated, the culture medium was replaced with 100 μl of Tyrode's solution containing various concentrations of the indicated drug/compound. The fluorescence intensities of the $GRAB_{DA}$ sensors were calibrated using mCherry as the reference.

Fluorescence imaging of $GRAB_{DA}$ in brain slices

Two weeks after the virus injection, the animals were anesthetized with Avetin and then decapitated. The brains were removed immediately and placed directly in cold slicing buffer containing (in mM): 110 choline-Cl, 2.5 KCl, 1.25 NaH_2PO_4, 25 $NaHCO_3$, 7 $MgCl_2$, 25 glucose, and 2 $CaCl_2$. The brains were then sectioned into 200-μm thick slices using a VT1200 vibratome (Leica, Germany), and the sections were transferred into the oxygenated Ringer's buffer containing (in mM): 125 NaCl, 2.5 KCl, 1.25 NaH_2PO_4, 25 $NaHCO_3$, 1.3 $MgCl_2$, 25 glucose, and 2 $CaCl_2$; the slices were then allowed to recover in 34 °C for at least 40 minutes. For fluorescence imaging, the slices were transferred to an imaging chamber in an Olympus FV1000MPE two-photon microscope equipped with a 40×/0.80 NA water-immersion objective and a mode-locked Mai Tai Ti:Sapphire laser (Spectra-Physics) tuned to 920 nm for the excitation of $GRAB_{DA}$ sensors and a 495~540 nm filter for signal collection. For electrical stimulation, a concentric electrode (model #CBAEC75, FHC) was positioned near the NAc core under the fluorescence guidance, and the imaging and stimulation were synchronized using an Arduino board with custom programs. The stimulation voltage was set at 5-6 V, and the duration of each stimulation was set at 2 ms.

For immunostaining of brain sections, $GRAB_{DA}$-expressing mice were anesthetized with Avetin, and the heart was perfused with 0.9% NaCl followed with 4% paraformaldehyde (PFA). The brain was then removed and placed in 4% PFA for 4 hours, then cryoprotected in 30% (w/v) sucrose for 24 hours. The brain was embedded into tissue-freezing medium, and 50-μm-thick coronal sections were cut using a Leica CM1900 cryostat (Leica, Germany). To label dopaminergic terminals and $GRAB_{DA}$ in the NAc, tissue sections were rinsed and then immunostained with rabbit anti-TH antibody (1:100, Millipore, #ab152) and chicken anti-GFP antibody (1:500, Abcam, #ab13970), followed by an Alexa-555-conjugated goat-anti-rabbit and Alexa-488-conjugated goat-anti-chicken secondary antibodies. The immunostained tissue sections were imaged using the same Nikon confocal microscope in cell imaging.

Fluorescence imaging of transgenic flies

Adult *Drosophila* (within 3 weeks of eclosion) were used for imaging

experiments. The mounting and dissection protocols were as previously described (Liang et al., 2013). In brief, a section of rectangular cuticle between the eyes was removed to expose the brain, which was then bathed in saline, so called adult hemolymph-like solution (AHLS). The same Olympus two-photon microscope used for brain slices imaging was also used here. For $GRAB_{DA}$ sensors imaging, 920-nm excitation laser and 495~540-nm filter were used. For jRCaMP1a, 1000-nm excitation laser and 575~630-nm filter were used. For olfactory stimulation, the odorant isoamyl acetate (Sigma-Aldrich; Cat. #306967) was firstly diluted 200-fold in mineral oil in a bottle; this dilution was subsequently diluted 5-fold in air, which was then delivered to the fly's antenna at a rate of 1000 ml/min. Compounds such as Halo and cocaine were added directly to the AHLS to their final concentration, and the following experiments were performed 10 min after compound application. For electrical stimulation, a glass electrode (resistance ~0.2 MΩ) was placed in the region of the DANs in the MB and the stimulation voltage was set at 20~80 V. Arduino was used to synchronized stimulation delivery and imaging with custom code. The sampling rates during olfactory stimulation and electrical stimulation was 2.7 Hz and 12 Hz, respectively.

Fluorescence imaging and chemogenetics in zebrafish

All experiments were performed on 5 days-post-fertilization (5 dpf) larvae in 10% Hank's solution containing (in mM): 140 NaCl, 5.4 KCl, 0.25 Na_2HPO_4, 0.44 KH_2PO_4, 1.3 $CaCl_2$, 1.0 $MgSO_4$, and 4.2 $NaHCO_3$ (pH 7.2). Imaging of Tg (elval3:$GRAB_{DA1m}$/DAT:TRPV1-TagRFP) larvae at 5 dpf was performed with an inverted confocal microscope (Olympus FV3000, Japan) using a 30X oil-immersion objective (1.05 N.A., morphology imaging) or an upright confocal microscope (Olympus FV1000, Japan) using 40X water-immersion objective (0.8 NA, time-lapse imaging). After the larvae were paralyzed with α-bungarotoxin (100 μg/ml, Sigma), they were mounted dorsal side up in 1.5% low melting-point agarose (Sigma) and then immersed in an extracellular solution consisting of (in mM): 134 NaCl, 2.9 KCl, 4 $CaCl_2$, 10 HEPES and 10 glucose (290 mOsmol/L, pH 7.8). For imaging the morphology, images were acquired with a field of view consisting of 1,024 pixels × 1,024 pixels with spatial resolution of 0.414 × 0.414 × 1 μm^3 (x × y × z). For bath application of compounds, dopamine (100 μM in 1 mM ascorbic acid solution, Sigma) was added by pipette at ~ 4 min and haloperidol (50 μM in DMSO, Tocris) at ~12 min. These images were acquired with a view field of 640 × 640 pixels with spatial resolution of 0.497 × 0.497 μm^2 (x × y) at ~1.5 Hz. For functional imaging,

small anterior dissections initiated in ventricles were made, after which a glass pipette containing the TRPV1 agonist capsaicin (50 μM in absolute ethanol, Tocris) was advanced through the incision and placed near the cell bodies of the DANs. To activate the DANs, 5 pulses of puffs (9-10 psi, 100-ms) were delivered with 1 min interval. The larvae were bath in Halo (50 μM in DMSO, Tocris) for 10 min before imaging. These images were acquired with a field of view consisting of 800 × 800 pixels with spatial resolution of 0.397 × 0.397 μm^2 (x × y) at ~1 Hz.

Fiber Photometry recording in freely moving mice

In all-optic experiments in Fig. 6, optical fiber probes (105 μm core /125 μm cladding) were implanted in the dorsal striatum and in SNc 4 weeks after the virus injection. Fiber photometry recording in the dorsal striatum was performed using a 50-μW 470-nm LED, and C1V1 in the SNc was stimulated using a 9.9-mW 561-nm laser. The measured emission spectra of $GRAB_{DA1m}$ and tdTomato were fitted using a linear unmixing algorithm https://www.niehs.nih.gov/research/atniehs/labs/ln/pi/iv/tools/index.cfm. The coefficients of $GRAB_{DA1m}$ and tdTomato generated by the unmixing algorithm were used to represent the fluorescence intensities of $GRAB_{DA1m}$ and tdTomato, respectively. To evoke C1V1-mediated DA release in the dorsal lateral striatum, pulse trains (10-ms pulses at 10 Hz for 1 s) were delivered to the SNc using a 9.9-mW, 561-nm laser. In other experiments in Fig. 7 and 8, an optic fiber (Thorlabs, FT200UMT,FT400UMT or BFH48-400) was attached to the implanted ferrule (Thorlabs, SF440-10) via a ceramic sleeve. A 400-Hz sinusoidal blue LED light (30 μW) (LED light: M470F1; LED driver: LEDD1B; both from Thorlabs) was bandpass filtered (passing band: 472 ± 15 nm, Semrock, FF02-472/30-25 in Fig.8 or 460-490nm in Fig.7) and delivered to the brain to excite $GRAB_{DA}$. The emission light then traveled through the same optic fiber, was bandpass filtered (passing band: 534 ± 25 nm, Semrock, FF01-535/50 in Fig.8 or 500-550nm in Fig.7), detected by a Femtowatt Silicon Photoreceiver (Newport, 2151) and recorded using a real-time processor (RZ5, TDT). The envelope of the 400-Hz signals that reflects the intensity of the fluorescence signals was extracted in real-time using a custom TDT program.

Behaviors

For the auditory conditioning task, mice were recovered for >3 days after surgery, and then water-restricted until reaching 85-90% of its original body weight and then prepared for behavior training. In the first Pavlovian task, the mice were trained on two frequency modulated pure tone auditory cues of 500 ms in duration, centered around 2.5 kHz and 11 kHz. For each mouse, one of the two tones was pseudo-randomly assigned to be the reward-predictive tone. Reward (water sweetened with 10% sucrose) was delivered through a water spout in front of the mouth following the reward-predictive cue with a variable 500-1500 ms delay. Rewarded and unrewarded trials were randomly interleaved with a variable inter-trial interval of 8-20 s. Mice experienced 200 trials (~100 rewards) per day in sessions lasting ~45 min.

In the subsequent Pavlovian conditioning task, the mice were trained on an auditory conditioning task, in which three pairs of auditory cues → outcomes pairs (or CS-US pairs; 8 kHz pure tone → 9 µl water; white noise → brief air puff to the face; and 2 kHz pure tone → no response) were delivered at random with a 10 -20 s randomized inter-trial interval. The duration and intensity of each auditory cue was 1 s and 70dB, respectively. The respective outcomes was delivered 1 s after the end of each auditory cue. The behavioral setup consisted of a custom-built apparatus allowing head fixation of the mouse's head to a Styrofoam rod (diameter: 15 cm). Rotation of the Styrofoam rod, which corresponds to the animal's running speed, was detected using an optical rotatory encoder. Licking behavior was detected when the mouse's tongue contacted the water delivery tube. Each lick signal was processed using an Arduino UNO board with custom code and sent digitally to the training program (written in MATLAB) via a serial port. Water delivery was precisely controlled using a stepping motor pump, and the air puff (15 psi, 25-ms duration) was controlled using a solenoid valve. Timing of the pump and valve was controlled using the same Arduino UNO board used for lick detection, which also provided synchronization between the training program and the data acquisition system (RZ2 processor, Tucker-Davis Technologies). During first two days of each training session, the outcomes were delivered without the prediction cues.

The sexual behaviors are defined following conventions in previous literature (Hull and Rodriguez-Manzo, 2009). In details, sniffing female was defined as the male's nose coming in close proximity to the female's facial, body, and/or urogenital areas. "Mount" was defined as when the male posed his forelegs over the female's back and with his hindfeet on the ground accompanying shallow pelvic thrusts. The mounting onset was defined as the moment at which

the male tried to clasp female back. “Intromission” was defined as a deep rhythmic thrust following mounting. The onset of intromission was defined as the time at which the male performed the first deep thrusting toward the female with vaginal penetration. “Penile grooming” was defined when a male animal repeated grooming for his urogenital area after intromission and ejaculation. Ejaculation is detected when the male stopped thrusting and freeze for seconds. The putative ejaculation event was confirmed by the presence of vaginal copulatory plug.

Data analysis

For imaging experiments in HEK293T cells, neurons, acute brain slices and transgenic flies, images were first analyzed using Image J software (National Institutes of Health), and then analyzed using Origin 9.1 (OriginLab) and MATLAB (MathWorks) with custom-written scripts. The data in acute brain slices and flies were first binned by 2x and averaged to generate representative traces.

For fiber photometry data, the signal baseline was first obtained by the MATLAB function “msbackadj” with a moving window of 25% of the total recording duration in Fig.8, or by subtracting 2nd order exponential fitted data from the raw data after 10.17 Hz binning in Fig. 7. The fluorescence responses were indicated by $\Delta F/F_0$ in Fig.8, which was calculated as $(F_{raw} - F_{baseline})/F_{baseline}$, or by Z score in Fig.7. To analyze event-evoked changes in DA release, we aligned each trial to the onset or offset of the behavior, and calculated the peri-stimulus time histogram (PSTH). To compare PSTH changes during different phases of the training, we used data from the 2nd day as naive, the 5-10th day as trained and >10th day as well-trained, and normalized the PSTH of each animal by water-evoked response during early training. The peak response during a behavior was calculated as the maximum $\Delta F/F_0$ during the behavior minus the average $\Delta F/F_0$ in the duration-matched period 2s prior to the behavior onset in Fig.8. The response to the CS was defined as the peak of the normalized PSTH between the CS onset and the US onset, and the response to US was calculated similarly using data from the US onset to data collected 2 s after the US onset in Fig.7.

Except where indicated otherwise, group differences were analyzed using the Student’s *t*-test, test, sign-rank test, One-Way ANOVA or post-hoc Tukey's test.

Except where indicated otherwise, all summary data presented as the mean ± SEM.

Acknowledgements

This work was supported by the National Basic Research Program of China (973 Program; grant 2015CB856402), the General Program of National Natural Science Foundation of China (project 31671118 and project 31371442), an NIH brain initiative grant NS103558, and the Junior Thousand Talents Program of China to Y.Li and to S.Zhang. Additional support was provided by the Ministry of Science and Technology of the People's Republic of China (2017YFA0505703) to M.Xu. We thank Y. Rao for sharing the 2-photon microscope and X. Lei for the platform support of Opera Phenix high content screening system at PKU-CLS. We thank the sequencing platform in the School of Life Sciences of Peking University. We thank R. Mooney, Y. Huan and L. Luo for valuable feedback of the manuscript.

Author Contributions

Y.L. conceived and supervised the project. F.S., M.J., and J.Z. performed experiments related to sensor development, optimization and characterization in culture HEK cells, culture neurons, brain slices and transgenic flies, with the initial work from YC. L. and J. F., and help from Z.Y.. F.L. and J.D. designed and performed experiments on transgenic fish. J.Z., Y.G., T.Y., W.P., S.O., L.W., S.Z., D.L., M.X., A.K., and G.C. designed and performed experiments in behaving mice. All authors contributed to data interpretation and data analysis. Y.L. wrote the manuscript with input from F.S., J.Z., M.J., D.L., S.O., M.X. and help from other authors.

References

Abercrombie, E.D., Keefe, K.A., DiFrischia, D.S., and Zigmond, M.J. (1989). Differential effect of stress on in vivo dopamine release in striatum, nucleus accumbens, and medial frontal cortex. Journal of neurochemistry *52*, 1655-1658.

Aso, Y., and Rubin, G.M. (2016). Dopaminergic neurons write and update memories with cell-type-specific rules. Elife *5*.

Aso, Y., Siwanowicz, I., Bracker, L., Ito, K., Kitamoto, T., and Tanimoto, H. (2010). Specific dopaminergic neurons for the formation of labile aversive memory. Current biology : CB *20*, 1445-1451.

Bainton, R.J., Tsai, L.T., Singh, C.M., Moore, M.S., Neckameyer, W.S., and Heberlein, U. (2000). Dopamine modulates acute responses to cocaine, nicotine and ethanol in Drosophila. Curr Biol *10*, 187-194.

1004 Balleine, B.W., Delgado, M.R., and Hikosaka, O. (2007). The role of the dorsal striatum in reward and
1005 decision-making. The Journal of neuroscience : the official journal of the Society for Neuroscience *27*,
1006 8161-8165.
1007 Barnea, G., Strapps, W., Herrada, G., Berman, Y., Ong, J., Kloss, B., Axel, R., and Lee, K.J. (2008). The
1008 genetic design of signaling cascades to record receptor activation. Proceedings of the National Academy
1009 of Sciences *105*, 64-69.
1010 Bayer, H.M., and Glimcher, P.W. (2005). Midbrain dopamine neurons encode a quantitative reward
1011 prediction error signal. Neuron *47*, 129-141.
1012 Beaulieu, J.M., and Gainetdinov, R.R. (2011). The physiology, signaling, and pharmacology of dopamine
1013 receptors. Pharmacol Rev *63*, 182-217.
1014 Berridge, K.C., and Robinson, T.E. (1998). What is the role of dopamine in reward: Hedonic impact,
1015 reward learning, or incentive salience? , pp. 309-369.
1016 Brooks, A.M., and Berns, G.S. (2013). Aversive stimuli and loss in the mesocorticolimbic dopamine
1017 system, pp. 281-286.
1018 Burke, C.J., Huetteroth, W., Owald, D., Perisse, E., Krashes, M.J., Das, G., Gohl, D., Silies, M., Certel, S.,
1019 and Waddell, S. (2012). Layered reward signalling through octopamine and dopamine in Drosophila.
1020 Nature *492*, 433-437.
1021 Burns, D.L. (1988). Subunit structure and enzymic activity of pertussis toxin. Microbiol Sci *5*, 285-287.
1022 Chien, E.Y.T., Liu, W., Zhao, Q., Katritch, V., Han, G.W., Hanson, M.A., Shi, L., Newman, A.H., Javitch, J.A.,
1023 and Cherezov, V. (2010a). Structure of the human dopamine D3 receptor in complex with a D2/D3
1024 selective antagonist. Science *330*, 1091-1095.
1025 Chien, E.Y.T., Liu, W., Zhao, Q., Katritch, V., Han, G.W., Hanson, M.A., Shi, L., Newman, A.H., Javitch, J.A.,
1026 Cherezov, V.*, et al.* (2010b). Structure of the human dopamine D3 receptor in complex with a D2/D3
1027 selective antagonist. Science (New York, NY) *330*, 1091-1095.
1028 Cichewicz, K., Garren, E., Adiele, C., Aso, Y., Wang, Z., Wu, M., Birman, S., Rubin, G., and Hirsh, J. (2017).
1029 A new brain dopamine‐deficient Drosophila and its pharmacological and genetic rescue. Genes, Brain
1030 and Behavior *16*, 394-403.
1031 Cognigni, P., Felsenberg, J., and Waddell, S. (2017). Do the right thing: neural network mechanisms of
1032 memory formation, expression and update in Drosophila. Curr Opin Neurobiol *49*, 51-58.
1033 Cohn, R., Morantte, I., and Ruta, V. (2015). Coordinated and compartmentalized neuromodulation
1034 shapes sensory processing in Drosophila. Cell *163*, 1742-1755.
1035 Cook Jr, E.H., Stein, M.A., Krasowski, M.D., Cox, N.J., Olkon, D.M., Kieffer, J.E., and Leventhal, B.L. (1995).
1036 Association of attention-deficit disorder and the dopamine transporter gene. American journal of
1037 human genetics *56*, 993.
1038 Da Silva, J.A., Tecuapetla, F., Paixão, V., and Costa, R.M. (2018). Dopamine neuron activity before action
1039 initiation gates and invigorates future movements. Nature *554*, 244-248.
1040 Damsma, G., Pfaus, J.G., Wenkstern, D., Phillips, A.G., and Fibiger, H.C. (1992). Sexual Behavior Increases
1041 Dopamine Transmission in the Nucleus Accumbens and Striatum of Male Rats: Comparison With
1042 Novelty and Locomotion. Behavioral Neuroscience *106*, 181-191.
1043 Daw, N.D., and Tobler, P.N. (2013). Value Learning through Reinforcement: The Basics of Dopamine and
1044 Reinforcement Learning. In, pp. 283-298.
1045 Di Chiara, G., and Imperato, A. (1988). Drugs abused by humans preferentially increase synaptic
1046 dopamine concentrations in the mesolimbic system of freely moving rats. Proc Natl Acad Sci U S A *85*,
1047 5274-5278.

1048 Fox, M.E., and Wightman, R.M. (2016). Contrasting Regulation of Catecholamine Neurotransmission in
1049 the Behaving Brain: Pharmacological Insights from an Electrochemical Perspective. Pharmacological
1050 reviews *69*, 12-32.
1051 Gibson, D.G., Young, L., Chuang, R.Y., Venter, J.C., Rd, H.C., and Smith, H.O. (2009). Enzymatic assembly
1052 of DNA molecules up to several hundred kilobases. Nature Methods *6*, 343.
1053 Giros, B., Jaber, M., Jones, S.R., Wightman, R.M., and Caron, M.G. (1996). Hyperlocomotion and
1054 indifference to cocaine and amphetamine in mice lacking the dopamine transporter. Nature *379*, 606-
1055 612.
1056 Glimcher, P.W. (2011). Understanding dopamine and reinforcement learning: The dopamine reward
1057 prediction error hypothesis. Proceedings of the National Academy of Sciences *108*, 15647-15654.
1058 Gonzales, R.A., Job, M.O., and Doyon, W.M. (2004). The role of mesolimbic dopamine in the
1059 development and maintenance of ethanol reinforcement, pp. 121-146.
1060 Graybiel, A.M., Aosaki, T., Flaherty, A.W., and Kimura, M. (1994). The basal ganglia and adaptive motor
1061 control. Science *265*, 1826-1831.
1062 Gunaydin, L.A., Grosenick, L., Finkelstein, J.C., Kauvar, I.V., Fenno, L.E., Adhikari, A., Lammel, S.,
1063 Mirzabekov, J.J., Airan, R.D., Zalocusky, K.A.*, et al.* (2014). Natural neural projection dynamics underlying
1064 social behavior. Cell *157*, 1535-1551.
1065 Hancock, J.F., Cadwallader, K., Paterson, H., and Marshall, C.J. (1991). A CAAX or a CAAL motif and a
1066 second signal are sufficient for plasma membrane targeting of ras proteins. The EMBO journal *10*, 4033-
1067 4039.
1068 Heisenberg, M. (2003). Mushroom body memoir: from maps to models. Nat Rev Neurosci *4*, 266-275.
1069 Hernandez, L., and Hoebel, B.G. (1988). Food reward and cocaine increase extracellular dopamine in
1070 the nucleus accumbens as measured by microdialysis. Life sciences *42*, 1705-1712.
1071 Holroyd, C.B., and Coles, M.G.H. (2002). The neural basis of human error processing: reinforcement
1072 learning, dopamine, and the error-related negativity. Psychol Rev *109*, 679-709.
1073 Howe, M.W., and Dombeck, D.A. (2016). Rapid signalling in distinct dopaminergic axons during
1074 locomotion and reward. Nature *535*, 505-510.
1075 Howes, O.D., and Kapur, S. (2009). The dopamine hypothesis of schizophrenia: version III—the final
1076 common pathway. Schizophrenia bulletin *35*, 549-562.
1077 Hull, E.M., and Rodriguez-Manzo, G. (2009). Male sexual behavior. Hormones, Brain and Behavior *1*, 5-
1078 65.
1079 Hung, L.W., Neuner, S., Polepalli, J.S., Beier, K.T., Wright, M., Walsh, J.J., Lewis, E.M., Luo, L., Deisseroth,
1080 K., Dölen, G.*, et al.* (2017). Gating of social reward by oxytocin in the ventral tegmental area. Science
1081 *357*, 1406-1411.
1082 Inagaki, H.K., de-Leon, S.B.-T., Wong, A.M., Jagadish, S., Ishimoto, H., Barnea, G., Kitamoto, T., Axel, R.,
1083 and Anderson, D.J. (2012). Visualizing neuromodulation in vivo: TANGO-mapping of dopamine signaling
1084 reveals appetite control of sugar sensing. Cell *148*, 583-595.
1085 Jaquins-Gerstl, A., and Michael, A.C. (2015). A review of the effects of FSCV and microdialysis
1086 measurements on dopamine release in the surrounding tissue. Analyst *140*, 3696-3708.
1087 Kim, M.W., Wang, W., Sanchez, M.I., Coukos, R., Von Zastrow, M., and Ting, A.Y. (2017). Time-gated
1088 detection of protein-protein interactions with transcriptional readout. eLife *6*.
1089 Kruse, A.C., Ring, A.M., Manglik, A., Hu, J., Hu, K., Eitel, K., Hã¼Bner, H., Pardon, E., Valant, C., and Sexton,
1090 P.M. (2013). Activation and allosteric modulation of a muscarinic acetylcholine receptor. Nature *504*,
1091 101-106.

1092 Kume, K., Kume, S., Park, S.K., Hirsh, J., and Jackson, F.R. (2005). Dopamine is a regulator of arousal in
1093 the fruit fly. Journal of Neuroscience *25*, 7377-7384.
1094 Lammel, S., Lim, B.K., and Malenka, R.C. (2014). Reward and aversion in a heterogeneous midbrain
1095 dopamine system. Neuropharmacology *76*, 351-359.
1096 Lanau, F., Zenner, M.-t., Civelli, O., and Hartman, D.S. (1997a). Epinephrine and Norepinephrine Act as
1097 Potent Agonists at the Recombinant Human Dopamine D4 Receptor.
1098 Lanau, F., Zenner, M.T., Civelli, O., and Hartman, D.S. (1997b). Epinephrine and norepinephrine act as
1099 potent agonists at the recombinant human dopamine D4 receptor. Journal of Neurochemistry *68*, 804-
1100 812.
1101 Lee, D., Creed, M., Jung, K., Stefanelli, T., Wendler, D.J., Oh, W.C., Mignocchi, N.L., Lüscher, C., and Kwon,
1102 H.-B. (2017). Temporally precise labeling and control of neuromodulatory circuits in the mammalian
1103 brain. Nature methods *14*, 495.
1104 Levitzki, A. (1988). From epinephrine to cyclic AMP. Science *241*, 800-806.
1105 Liang, L., Li, Y., Potter, C.J., Yizhar, O., Deisseroth, K., Tsien, R.W., and Luo, L. (2013). GABAergic projection
1106 neurons route selective olfactory inputs to specific higher-order neurons. Neuron *79*, 917-931.
1107 Liu, C., Placais, P.Y., Yamagata, N., Pfeiffer, B.D., Aso, Y., Friedrich, A.B., Siwanowicz, I., Rubin, G.M., Preat,
1108 T., and Tanimoto, H. (2012). A subset of dopamine neurons signals reward for odour memory in
1109 Drosophila. Nature *488*, 512-516.
1110 Lohse, M.J., Hein, P., Hoffmann, C., Nikolaev, V.O., Vilardaga, J.P., and Bunemann, M. (2008). Kinetics of
1111 G-protein-coupled receptor signals in intact cells. Br J Pharmacol *153 Suppl 1*, S125-132.
1112 Lotharius, J., and Brundin, P. (2002). Pathogenesis of Parkinson's disease: dopamine, vesicles and α-
1113 synuclein. Nature Reviews Neuroscience *3*, 932.
1114 Luttrell, L.M., and Lefkowitz, R.J. (2002). The role of beta-arrestins in the termination and transduction
1115 of G-protein-coupled receptor signals. J Cell Sci *115*, 455-465.
1116 Marvin, J.S., Borghuis, B.G., Tian, L., Cichon, J., Harnett, M.T., Akerboom, J., Gordus, A., Renninger, S.L.,
1117 Chen, T.-W., Bargmann, C.I., *et al.* (2013). An optimized fluorescent probe for visualizing glutamate
1118 neurotransmission. Nature methods *10*, 162-170.
1119 Mas, M., Fumero, B., and González-Mora, J. (1995). Voltammetric and microdialysis monitoring of brain
1120 monoamine neurotransmitter release during sociosexual interactions. Behavioural Brain Research *71*.
1121 Missale, C., Nash, S.R., Robinson, S.W., Jaber, M., and Caron, M.G. (1998). Dopamine receptors: from
1122 structure to function. Physiol Rev *78*, 189-225.
1123 Muller, A., Joseph, V., Slesinger, P.A., and Kleinfeld, D. (2014). Cell-based reporters reveal in vivo
1124 dynamics of dopamine and norepinephrine release in murine cortex. nAture methods *11*, 1245.
1125 Nair-Roberts, R.G., Chatelain-Badie, S.D., Benson, E., White-Cooper, H., Bolam, J.P., and Ungless, M.A.
1126 (2008). Stereological estimates of dopaminergic, GABAergic and glutamatergic neurons in the ventral
1127 tegmental area, substantia nigra and retrorubral field in the rat. Neuroscience *152*, 1024-1031.
1128 Neves, S.R., Ram, P.T., and Iyengar, R. (2002). G protein pathways, pp. 1636-1639.
1129 Nieoullon, A. (2002). Dopamine and the regulation of cognition and attention. Progress in neurobiology
1130 *67*, 53-83.
1131 Park, J., Kile, B.M., and Wightman, M.R. (2009). In vivo voltammetric monitoring of norepinephrine
1132 release in the rat ventral bed nucleus of the stria terminalis and anteroventral thalamic nucleus.
1133 European Journal of Neuroscience *30*, 2121-2133.
1134 Pfaus, J.G., Damsma, G., Nomikos, G.G., Wenkstern, D.G., Blaha, C.D., Phillips, A.G., and Fibiger, H.C.
1135 (1990a). Sexual behavior enhances central dopamine transmission in the male rat. Brain Res *530*, 345-

348.

Pfaus, J.G., Damsma, G., Nomikos, G.G., Wenkstern, D.G., Blaha, C.D., Phillips, A.G., and Fibiger, H.C. (1990b). Sexual behavior enhances central dopamine transmission in the male rat. Brain Research *530*, 345-348.

Pfeiffer, B.D., Truman, J.W., and Rubin, G.M. (2012). Using translational enhancers to increase transgene expression in Drosophila. Proceedings of the National Academy of Sciences *109*, 6626-6631.

Pignatelli, M., and Bonci, A. (2015). Role of Dopamine Neurons in Reward and Aversion: A Synaptic Plasticity Perspective. Neuron *86*, 1145-1157.

Rasmussen, S.G.F., DeVree, B.T., Zou, Y., Kruse, A.C., Chung, K.Y., Kobilka, T.S., Thian, F.S., Chae, P.S., Pardon, E., Calinski, D.*, et al.* (2011). Crystal structure of the β2 adrenergic receptor–Gs protein complex. Nature *477*, 549-555.

Ritz, M.C., Lamb, R., and Kuhar, M. (1987). Cocaine receptors on dopamine transporters are related to self-administration of cocaine. Science *237*, 1219-1223.

Robinson, D.L., Heien, M.L.a.V., and Wightman, R.M. (2002). Frequency of dopamine concentration transients increases in dorsal and ventral striatum of male rats during introduction of conspecifics. The Journal of neuroscience : the official journal of the Society for Neuroscience *22*, 10477-10486.

Robinson, D.L., Hermans, A., Seipel, A.T., and Wightman, R.M. (2008). Monitoring rapid chemical communication in the brain. Chem Rev *108*, 2554-2584.

Robinson, D.L., Phillips, P.E.M., Budygin, E.A., Trafton, B.J., Garris, P.A., and Wightman, R.M. (2001). Sub-second changes in accumbal dopamine during sexual behavior in male rats. NeuroReport *12*, 2549-2552.

Robinson, D.L., Venton, B.J., Heien, M.L., and Wightman, R.M. (2003). Detecting subsecond dopamine release with fast-scan cyclic voltammetry in vivo. Clin Chem *49*, 1763-1773.

Rodeberg, N.T., Sandberg, S.G., Johnson, J.A., Phillips, P.E., and Wightman, R.M. (2017). Hitchhiker's guide to voltammetry: acute and chronic electrodes for in vivo fast-scan cyclic voltammetry. ACS chemical neuroscience *8*, 221-234.

Sanchez-Soto, M., Bonifazi, A., Cai, N.S., Ellenberger, M.P., Newman, A.H., Ferre, S., and Yano, H. (2016). Evidence for Noncanonical Neurotransmitter Activation: Norepinephrine as a Dopamine D2-Like Receptor Agonist. Molecular pharmacology *89*, 457-466.

Schultz, W. (2006). Behavioral theories and the neurophysiology of reward. Annual review of psychology *57*, 87-115.

Schultz, W. (2007). Behavioral dopamine signals, pp. 203-210.

Schultz, W. (2016). Dopamine reward prediction-error signalling: a two-component response. Nature Reviews Neuroscience *17*, 183.

Schultz, W., Dayan, P., and Montague, P.R. (1997). A neural substrate of prediction and reward. Science *275*, 1593-1599.

Schwaerzel, M., Monastirioti, M., Scholz, H., Friggi-Grelin, F., Birman, S., and Heisenberg, M. (2003). Dopamine and octopamine differentiate between aversive and appetitive olfactory memories in Drosophila. J Neurosci *23*, 10495-10502.

Shang, C.F., Li, X.Q., Yin, C., Liu, B., Wang, Y.F., Zhou, Z., and Du, J.L. (2015). Amperometric Monitoring of Sensory-Evoked Dopamine Release in Awake Larval Zebrafish. J Neurosci *35*, 15291-15294.

Sokoloff, P., Giros, B., Martres, M.-P., Bouthenet, M.-L., and Schwartz, J.-C. (1990). Molecular cloning and characterization of a novel dopamine receptor (D3) as a target for neuroleptics. Nature *347*, 146-151.

Sung, Y.M., Wilkins, A.D., Rodriguez, G.J., Wensel, T.G., and Lichtarge, O. (2016). Intramolecular allosteric communication in dopamine D2 receptor revealed by evolutionary amino acid covariation. Proceedings

of the National Academy of Sciences of the United States of America *113*, 3539.

Tidey, J.W., and Miczek, K.A. (1996). Social defeat stress selectively alters mesocorticolimbic dopamine release: an in vivo microdialysis study. Brain Res *721*, 140-149.

Ungless, M.A., and Grace, A.A. (2012). Are you or aren't you? Challenges associated with physiologically identifying dopamine neurons. Trends in neurosciences *35*, 422-430.

Ungless, M.A., Magill, P.J., and Bolam, J.P. (2004). Uniform inhibition of dopamine neurons in the ventral tegmental area by aversive stimuli. Science *303*, 2040-2042.

van Erp, A.M., and Miczek, K.A. (2000). Aggressive behavior, increased accumbal dopamine, and decreased cortical serotonin in rats. J Neurosci *20*, 9320-9325.

Vilardaga, J.-P., Bünemann, M., Krasel, C., Castro, M., and Lohse, M.J. (2003). Measurement of the millisecond activation switch of G protein-coupled receptors in living cells. Nature biotechnology *21*, 807-812.

Volkow, N.D., Wang, G.J., Fowler, J.S., Fischman, M., Foltin, R., Abumrad, N.N., Gatley, S.J., Logan, J., Wong, C., Gifford, A.*, et al.* (1999). Methylphenidate and cocaine have a similar in vivo potency to block dopamine transporters in the human brain. Life Sciences *65*.

Wang, S., Che, T., Levit, A., Shoichet, B.K., Wacker, D., and Roth, B.L. (2018). Structure of the D₂ dopamine receptor bound to the atypical antipsychotic drug risperidone. Nature 2018, 1-24.

Wang, S., Wacker, D., Levit, A., Che, T., Betz, R.M., Mccorvy, J.D., Venkatakrishnan, A.J., Huang, X.P., Dror, R.O., and Shoichet, B.K. (2017). D4 dopamine receptor high-resolution structures enable the discovery of selective agonists. Science *358*, 381-386.

Wise, R.A. (2004). Dopamine, learning and motivation. Nature reviews neuroscience *5*, 483.

Wisor, J.P., Nishino, S., Sora, I., Uhl, G.H., Mignot, E., and Edgar, D.M. (2001). Dopaminergic role in stimulant-induced wakefulness. Journal of Neuroscience *21*, 1787-1794.

Yizhar, O., Fenno, L.E., Prigge, M., Schneider, F., Davidson, T.J., Ogshea, D.J., Sohal, V.S., Goshen, I., Finkelstein, J., Paz, J.T.*, et al.* (2011). Neocortical excitation/inhibition balance in information processing and social dysfunction. Nature *477*, 171-178.

Zhang, Q., Li, Y., and Tsien, R.W. (2009). The Dynamic Control of Kiss-And-Run. Science *000858*, 1448-1453.

Ziegler, N., Batz, J., Zabel, U., Lohse, M.J., and Hoffmann, C. (2011). FRET-based sensors for the human M1-, M3-, and M5-acetylcholine receptors. Bioorg Med Chem *19*, 1048-1054.

Figure 1. Design, optimization and characterization of $GRAB_{DA}$ sensors in cultured HEK293T cells.

(A-C) Schematic diagrams showing the strategy used to develop $GRAB_{DA}$ sensors (top panels), and the corresponding performance of each variants in each optimization step (bottom panels).

(A) Optimization of the cpEGFP insertion site within the third intracellular loop (ICL3) in D_2R. The $\Delta F/F_0$ of $GRAB_{DA}$-expressing cells in response to 100 μM DA application is shown below. $GRAB_{DA1m}$, with the highest $\Delta F/F_0$ (~90%), was selected for further optimization. Each data point represents the average of 3-5 cells.

(B) Optimization of the linkers between the D_2R and cpEGFP. Mutants were generated by changing each linker residue to 20 possible amino acids. The $\Delta F/F_0$ of the $GRAB_{DA}$-expressing cells relative to the brightness in response to 100 μM DA application is shown below. Each data point represents the average of 100-400 cells.

(C) Affinity tuning. Either the T205M single mutation, or the C118A/S193N double mutations, were introduced into $GRAB_{DA}$, and the normalized dose-dependent fluorescence responses of various $GRAB_{DA}$-expressing cells in response to DA application are plotted below. Each data point represents average of 6 wells containing 100-400 cells per well.

(D-E) Fluorescence changes in $GRAB_{DA}$ -expressing cells in response to 100 μM DA followed by 10 μM Halo. Peak $\Delta F/F_0$ values in response to DA are summarized in the right panel in (E) ($GRAB_{DA1m}$: n = 18 cells from 4 cultures (18/4); $GRAB_{DA1m\text{-}mut}$: n = 15/3; $GRAB_{DA1h}$: n = 14/3; $GRAB_{DA1h\text{-}mut}$: n = 14/3; $p < 0.001$ between DA1m and DA1m-mut; $p < 0.001$ between DA1h and DA1h-mut; $p = 0.42$ between DA1m and DA1h).

(F) Schematic image showing the local perfusion system. A glass pipette (black dashed lines) filled with DA or Halo was positioned close to the $GRAB_{DA}$-expressing cells, and fluorescence was measured using confocal line-scanning (red line).

(G) Left and middle: fluorescence changes in $GRAB_{DA}$-expressing cells in response to the local perfusion (on rate: 100 μM DA in pipette with normal bath solution; off rate: 1 mM Halo in pipette with bath solution containing 10 μM DA for $GRAB_{DA1m}$ or 1 μM DA for $GRAB_{DA1h}$). The traces are the average of 3 different ROIs on the scanning line and are shaded with ± SEM. Right: group data summarizing the response kinetics of $GRAB_{DA}$-expressing cells in response to DA (on) or Halo (off) (n = 8/group; $p = 0.0093$ between on kinetics; $p < 0.001$ between off kinetics).

(H) Normalized fluorescence changes in $GRAB_{DA1m}$- and $GRAB_{DA1m\text{-}mut}$-expressing cells in response to the application of indicated compounds at 1 μM, including: DA, DA + Halo, DA + Etic, DA + SCH-23390 (SCH), norepinephrine (NE), 5-HT, histamine (His), glutamate (Glu), gamma-aminobutyric acid (GABA), adenosine (Ade), acetylcholine (ACh), tyramine (Tyr), octopamine (Oct), glycine (Gly), or L-DOPA (the first bar shows $GRAB_{DA1m\text{-}mut}$-expressing cells in response to DA; n = 4 wells per group with 200-400 cells per well; $p < 0.001$ for DA-induced responses between $GRAB_{DA1m}$ and $GRAB_{DA1m\text{-}mut}$; $p = 0.99$ for $GRAB_{DA1m}$ responses induced by DA comparing with DA+SCH; $p < 0.001$ for $GRAB_{DA1m}$ responses induced by DA comparing with DA+Halo, DA+Etic, NE, 5-HT, His, Glu, GABA, Ade, ACh, Tyr, Oct, Gly and L-DOPA). The inset shows the normalized dose-dependent fluorescence responses of $GRAB_{DA1m}$-expressing cells in response to DA (red) and NE (green) application (n = 6 wells per group with 100-300 cells per well; $p = 0.002$ at -7.5; $p < 0.001$ at -7, -6.5 and -6; $p = 0.007$ at -5).

(I) Normalized fluorescence changes in $GRAB_{DA}$-expressing cells in response to the application of DA, with or without the co-expression of pertussis toxin (PTX) ($GRAB_{DA1m}$: n = 14/3; $GRAB_{DA1m}$+PTX: n = 14/3; $GRAB_{DA1h}$: n = 10/3; $GRAB_{DA1h}$+PTX: n = 10/3; $p = 0.680$ comparing the EC_{50} of $GRAB_{DA1m}$ and $GRAB_{DA1m}$ +PTX; $p = 0.810$ for comparing the EC_{50} of $GRAB_{DA1h}$ and $GRAB_{DA1h}$ +PTX).

(J) Normalized Fluorescence changes in $GRAB_{DA}$-expressing cells during a 2-hour application of 100 μM DA (n = 3 wells/group; $p = 0.620$ for $GRAB_{DA1m}$; $p = 0.792$ for $GRAB_{DA1h}$).

Scale bars, 10 μm in (D) and (F).

Values with error bars indicate mean ± SEM.

Students' t-test performed; n.s., not significant; **, $p < 0.01$; ***, $p < 0.001$.

See also Fig. S1-S3.

Figure 2. Characterization of $GRAB_{DA}$ sensors in cultured neurons.

(A) Expression of $GRAB_{DA}$ sensors in cultured neurons. Scale bars, 20 μm.

(B) Expression and localization of $GRAB_{DA}$ sensors (green, G), subcellular markers (red, R) and overlay (O) in the indicated subcellular compartments in cultured neurons. RFP-CAAX, PSD95-RFP and Synaptophysin-RFP were co-expressed as markers of the plasma membrane, dendritic spines, and presynaptic boutons, respectively. Scale bars, 5 μm.

(C and D) Fluorescence changes in $GRAB_{DA}$-expressing neurons in response to the application of 100 μM DA followed by 10 μM Halo. Scale bars, 30 μm ($GRAB_{DA1m}$: n = 13/7; $GRAB_{DA1m\text{-}mut}$: n = 14/5; $GRAB_{DA1h}$: n = 16/4; $GRAB_{DA1h\text{-}mut}$: n = 10/5; $p < 0.001$ between DA1m and DA1m-mut; $p < 0.001$ between DA1h and DA1h-mut; $p = 0.88$ between DA1m and DA1h).

(E) Time courses (left) and dose-dependent fluorescence changes (right) of $GRAB_{DA}$-expressing neurons in response to DA application ($GRAB_{DA1m}$: n = 10/6; $GRAB_{DA1m\text{-}mut}$: n = 6/6; $GRAB_{DA1h}$: n = 10/5; $GRAB_{DA1h\text{-}mut}$: n = 10/3).

(F) Fluorescence changes in $GRAB_{DA1m}$-expressing neurons in response to the transient application of the indicated compounds at 1 μM, including DA, L-Dopa, 5-HT, His, ACh, DA(2^{nd}) and DA+Halo (n = 12/12; $p < 0.001$ comparing responses in DA with that in L-Dopa, 5-HT, His, ACh and DA+Halo).

(G) Fluorescence changes in $GRAB_{DA}$-expressing neurons during a 2-hour application of 100 μM DA ($GRAB_{DA1m}$: n = 20/12; $GRAB_{DA1h}$: n = 14/6; $p = 0.085$ for DA1m; $p = 0.085$ for DA1h).

Values with error bars indicate mean ± SEM.

Student's t-test performed; n.s., not significant; ***, $p < 0.001$.

See also Fig. S4.

Figure 3. Release of endogenous DA measured in acute mouse brain slices.

(A) Left three panels, schematic diagrams of the viral expression vector, experimental protocol for expressing $GRAB_{DA}$ sensors and imaging DA dynamics in mouse brain slices containing NAc. Right, the immunoreactive signals of $GRAB_{DA}$ (green) expressed in NAc neurons and TH (red) in dopaminergic terminals. Scale bar, 100 μm.

(B) Representative traces (left and middle) and group analysis (right) of the fluorescence changes in $GRAB_{DA1m}$- and $GRAB_{DA1h}$-expressing neurons in response to a train of 20 Hz electrical stimuli containing the indicated pulse numbers. Each trace is the average of 3 separate trials in one slice ($GRAB_{DA1m}$: n = 5 slices from 3 mice; $GRAB_{DA1h}$: n = 7 slices from 4 mice).

(C) Similar as (B), except that a train of 10-pulse electrical stimuli was applied at the indicated frequencies ($GRAB_{DA1m}$: n = 3 slices from 2 mice; $GRAB_{DA1h}$: n = 8 slices from 4 mice).

(D) Representative traces (left) and group analysis (right) of the normalized fluorescence changes and kinetics in $GRAB_{DA1m}$- and $GRAB_{DA1h}$-expressing neurons in response to 10 electrical pulses delivered at 100 Hz. The rising (on) and decaying (off) phases in the traces were fitted separately, and the response time constants are summarized on the right ($GRAB_{DA1m}$: n = 3 slices from 2 mice; $GRAB_{DA1h}$: n = 5-8 slices from 3 mice).

(E) The fluorescence changes in $GRAB_{DA1m}$- and $GRAB_{DA1h}$-expressing neurons in response to multiple trains of electrical stimuli at an interval of 5 min. The fluorescence changes measured during the first train in each slice were used to normalize the data ($GRAB_{DA1m}$: n = 3 slices form 2 mice; $GRAB_{DA1h}$: n = 6 slices from 3 mice).

(F) Representative traces (left and middle) and group analysis (right) of the fluorescence changes in $GRAB_{DA1m}$- and $GRAB_{DA1h}$-expressing neurons in response to 20 electrical pulses (at 20 Hz), in control solution (ACSF) or solution containing 10 μM Halo ($GRAB_{DA1m}$: n = 5 slices from 4 mice, $p < 0.001$ comparing ACSF with Halo; $GRAB_{DA1h}$: n = 6 slices from 4 mice, $p < 0.001$ comparing ACSF with Halo).

Values with error bars indicate mean ± SEM.

The shaded areas and error bars indicate ± SEM.

Student's t-test performed; ***, $p < 0.001$.

Figure 4. *In vivo* imaging of DA dynamics in the *Drosophila* brain.

(A) Schematic illustration depicting the *in vivo* olfactory stimulation and imaging experiment under two-photon microscopy.

(B and C) Representative pseudo-color images and traces (B) and group analysis (C) of the fluorescence changes of TH > $GRAB_{DA1m}$ and TH > $GRAB_{DA1m\text{-}mut}$ flies in response to 1 s olfactory stimulation (TH > $GRAB_{DA1m}$: n = 12 flies; TH > $GRAB_{DA1m\text{-}mut}$: n = 5 flies; c305a > $GRAB_{DA1m}$ with WT background: n = 6 flies; c305a > $GRAB_{DA1m}$ with TH-deficient background: n = 6 flies; $p < 0.001$ for responses of TH > $GRAB_{DA1m}$ in saline comparing with Halo; $p < 0.001$ for responses of TH > $GRAB_{DA1m}$ in saline comparing with TH > $GRAB_{DA1m\text{-}mut}$ in saline; $p = 0.002$ for responses of c305a > $GRAB_{DA1m}$ with WT background comparing with TH-deficient background).

(D) Schematic illustrations depicting *in vivo* electrical stimulation experiment, in which the electrode was positioned near the $GRAB_{DA1m}$-expressing DANs in order to evoke DA release.

(E) Representative pseudo-color images of the fluorescence changes in TH > $GRAB_{DA1m}$ and TH > $GRAB_{DA1m\text{-}mut}$ flies in response to multiple trains of electrical stimuli. Shown below are single-trial traces (in gray) and 6-trial averaged traces (blue and black) measured in one fly with indicated genotypes. Each vertical tick indicates 1 ms electrical stimulation ("stim").

(F-I) Fluorescence changes in TH > $GRAB_{DA1m}$ flies in response to the indicated pulses of electrical stimuli (at 20 Hz), showing representative traces (F), group data for peak $\Delta F/F_0$ (G), integrated data (H) and the response kinetics (I) (n = 9 flies per group).

(J and K) Representative traces (J) and group analysis (K) of fluorescence changes in TH > $GRAB_{DA1m}$ and TH > $GRAB_{DA1m\text{-}mut}$ flies in response to 40 pulses electrical stimuli (at 20 Hz), in normal saline or in saline containing 10 μM Halo (TH > $GRAB_{DA1m}$: n = 5 flies; TH > $GRAB_{DA1m\text{-}mut}$: n = 5 flies; $p = 0.004$ for responses of TH > $GRAB_{DA1m}$ in saline comparing with Halo; $p = 0.007$ for responses of TH > $GRAB_{DA1m}$ in saline comparing with TH > $GRAB_{DA1m\text{-}mut}$ in saline).

(L-O) Fluorescence changes in TH > $GRAB_{DA1m}$ flies in response to 1 s olfactory stimulation, in control condition, in the presence of the DAT blocker cocaine (3 μM) or when the DAT expression in DAN was impaired by DAT-RNAi. Schematic illustration of the experimental design in (L). Representative traces (M) were fitted with a single-exponential function (red traces), with the decay time constants shown. The group analysis of integrated data and the decay time constants are shown in (N) and (O), respectively (TH > $GRAB_{DA1m}$: n = 10

flies; TH > $GRAB_{DA1m}$, DAT-RNAi: n = 11 flies; between control and cocaine groups, p = 0.002 for integrals and p = 0.025 for decay time constants; between control and DAT-RNAi groups, $p < 0.001$ for both integrals and decay time constants; between cocaine and DAT-RNAi groups, p = 0.095 for integrals and p = 0.053 for decay time constants).

The fluorescence traces in (B), (F), (J), and (M) are the averaged results of 3~6 trials from one fly, and the shaded area indicates ± SEM.

Values with error bars indicate mean ± SEM.

Student's t-test performed; n.s., not significant; *, $p < 0.05$; **, $p < 0.01$; ***, $p < 0.001$.

Scale bars in (B) and (E), 25 μm.

See also Fig. S5.

Figure 5. Monitoring *in vivo* DA release in transgenic zebrafish.

(A) Fluorescence images of a transgenic zebrafish larvae expressing $GRAB_{DA1m}$ (green) pan-neuronally and TRPV1-TagRFP (red) in DANs. Zoom-in view of $GRAB_{DA1m}$-expressing neurons in indicated brain regions are shown (left).

(B-D) Representative pseudo-color images (B), trace (C) and group analysis (D) of fluorescence changes of $GRAB_{DA1m}$-expressing neurons in response to 100 μM DA followed by 50 μM Halo (n = 6 fishes; p = 0.002 between DA and DA+Halo).

(E) Schematic diagram showing the experimental design to chemogenetically activate TRPV1-expressing DANs by capsaicin. The tectal neurons downstream of the DANs were analyzed as indicated by the region of interest (ROI).

(F) Representative traces of the fluorescence changes in $GRAB_{DA1m}$-expressing neurons in response to 5 pulses of 50 μM capsaicin (each vertical orange tick indicates 100-ms puffs of capsaicin with a 1 min interval) in control normal solution (green) or solution containing 50 μM Halo (blue).

(G and H) Averaged traces (G) and group analysis (H) of the fluorescence changes in $GRAB_{DA1m}$-expressing neurons in response to single trial of capsaicin application, in control normal solution (green) or solution containing 50 μM Halo (blue) (n = 5 fishes; p = 0.006 between control and Halo).

Scale bars in (A) and (B), 50 μm.

Paired student's t-test performed.

Figure 6. Striatal DA dynamics measured in freely moving mice during optogenetic stimulation of the SNc.

(A) Illustration depicting the experimental design with dual-color optical recordings of $GRAB_{DA1m}$- and tdTomato-expressing neurons in the dorsal striatum during simultaneous optogenetic stimulation of DANs in the SNc.

(B) A representative frame of the emission spectra of $GRAB_{DA1m}$ and tdTomato co-expressed in the dorsal striatum. The black trace shows the measured spectrum; the blue dashed trace shows the corresponding best fitting curve generated by a linear unmixing algorithm.

(C) Spontaneous DA fluctuations represented by the ratio of $GRAB_{DA1m}$ to tdTomato fluorescence in a freely moving mouse (top) and its representative traces in the control condition (bottom left), 5 min after the i.p. injection of DAT blocker methylphenidate (10 mg/kg, bottom middle), and 5 min after the i.p. injection of D_2R antagonist Etic (2 mg/kg, bottom right). Black lines above indicate the time of compound administration. Yellow ticks indicate the time of optogenetic stimulation.

(D) Averaged fluorescence changes (mean ± SEM, n = 20 trials from 4 hemispheres of 2 mice) of $GRAB_{DA1m}$ (green) in the dorsal striatum in response to optogenetic C1V1 stimulation of DANs in the SNc under indicated conditions: baseline (left), after the i.p. injection of methylphenidate (middle), and after the i.p. injection of Etic (right). The off kinetics were fitted with a single-exponential function (black traces).

(E) Comparison of the decay time constants of C1V1-evoked $GRAB_{DA1m}$ fluorescence responses between the control condition and after methylphenidate injection (n = 20 trials from 4 hemispheres of 2 mice).

(F) Comparison of the magnitude of C1V1-evoked $GRAB_{DA1m}$ fluorescence changes between the control condition and after Etic injection (n = 20 trials from 4 hemispheres of 2 mice).

***, $p < 0.001$, student's t-test performed in (E) and (F).

Figure 7. Dopamine release in NAc measured during various training phases of an auditory conditioning task.

(A) Recording configuration for head-fixed Pavlovian conditioning task. Dopamine dynamics in the NAc were monitored by recording the fluorescence changes in $GRAB_{DA}$-expressing neurons using fiber photometry.

(B) Exemplar trace from *in vivo* fiber photometry recording from a trained mouse expressing $GRAB_{DA1h}$ in NAc, encompassing four sequential trials. The timings of cues (CS) or water reward (US) are indicated above.

(C) Task-aligned photometry signals from an exemplar mouse in the first behavioral session aligned to the cue (CS, left) or to the reward delivery (US, right). Note robust reward-related signal and absence of cue-related signal.

(D) Task-aligned photometry signals from the same moues in (C) after training. Note emergence of DA response to reward-predictive cue.

(E) Group data demonstrating $GRAB_{DA1h}$ responses to water (US, left) or cue (CS, middle) in the NAc of both naïve and trained mice (n = 9 mice; US response: naïve N.W.: p = 0.084; naïve water: p = 0.0020; trained N.W.: p = 0.56; trained water: p = 0.0020; CS response: naïve N.W.: p = 0.37; naïve water: p = 1.0000; trained N.W.: p = 0.043; trained water: p = 0.0020, signed rank test performed).

(F) Direct comparison of baseline-subtracted cue responses reveals equivalent lack of response to N.W. or reward-predictive cue in naïve mice (left), and elevated response to reward-predictive cue over N.W. cue in trained mice (right). Baseline subtraction was performed trial-by-trial by comparing the cue response (100 ms – 1000 ms following onset of the cue) to 900 ms before onset of the cue. This cue response window encompassed the auditory cue as well as the variable delay period and terminated before the earliest reward delivery times (naïve: p = 0.43; trained: p = 0.0020, signed rank test performed).

(G) Representative fluorescence changes in $GRAB_{DA1m}$-expressing neurons in the NAc during training. The heat map shows the fluorescence changes in the first 50 consecutive trials in each category, with each trial time-aligned to the onset of the auditory cue. The lower panels show the post-event histograms (PSTH) from all trials; the shaded area indicates ± SD. The fluorescence changes measured during naïve, trained and well-trained phases in the same mouse are shown, respectively.

(H) Group analysis of the normalized peak z-scores for the US and CS in the indicated training phases. Each trace (coded with specific gray value) represents data from one animal (n = 3 mice; US: p = 0.7638 between naive

and trained, p = 0.0125 between naive and well-trained, p = 0.0080 between trained and well-trained; CS: p = 0.1032 between naive and trained, p = 0.0067 between naive and well-trained, p = 0.0471 between trained and well-trained). Error bars, ± SEM. Post-hoc Tukey's test was performed; n.s., not significant; *, $p < 0.05$; **, $p < 0.01$; ***, $p < 0.001$.

Figure 8. Acute DA release in the NAc measured during male sexual behaviors.

(A) Schematic diagram showing the experimental design used to record $GRAB_{DA1h}$ signals in the NAc of male mice during sexual behaviors.

(B) Representative fluorescence changes in male mice during the indicated sexual behaviors. The shaded areas with colors indicate different behavioral events.

(C) Post-event histogram (PETH) showing the $GRAB_{DA1h}$ signals aligned to the indicated behavioral events.

(D) Group data summarizing the average peak $\Delta F/F_0$ (baseline adjusted) during different indicated behaviors for the two mice shown in (C) (n = 2 mice; p = 0.007 for animal 1; $p < 0.001$ for animal 2). Error bars, ± SEM. One-way ANOVA performed; ***, $p < 0.001$; **, $p < 0.01$.

Figure 1

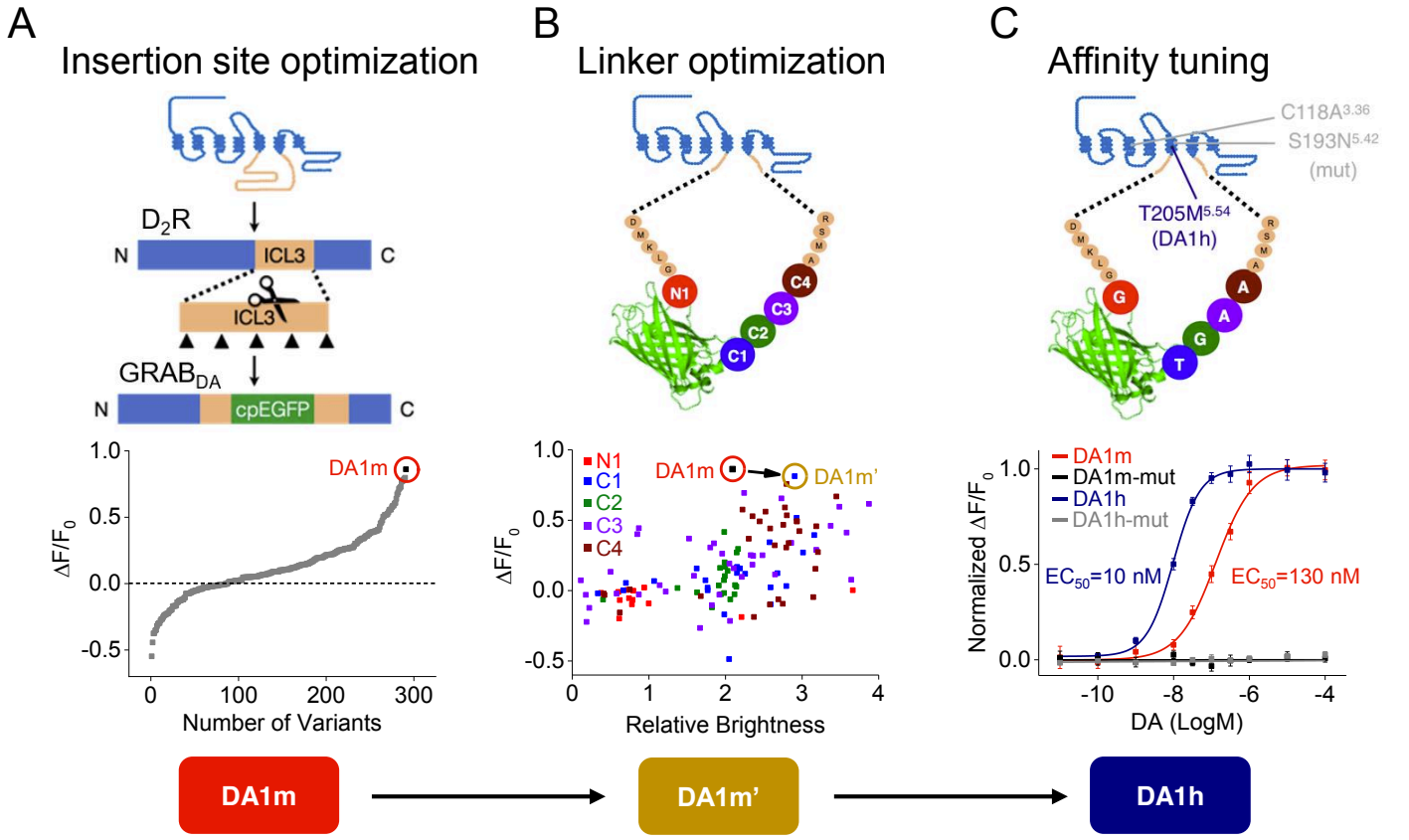

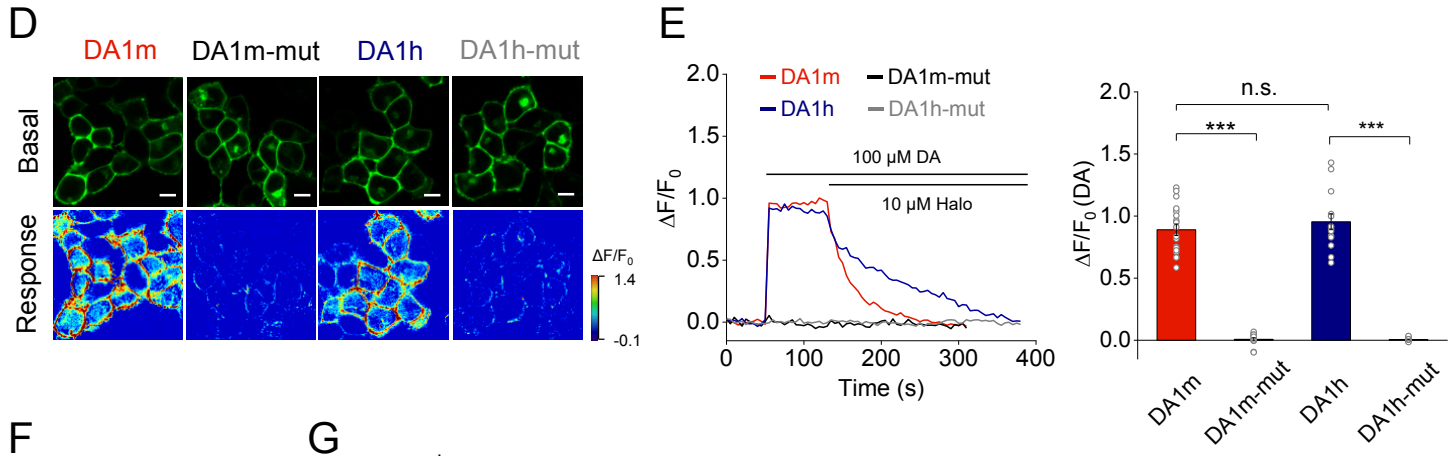

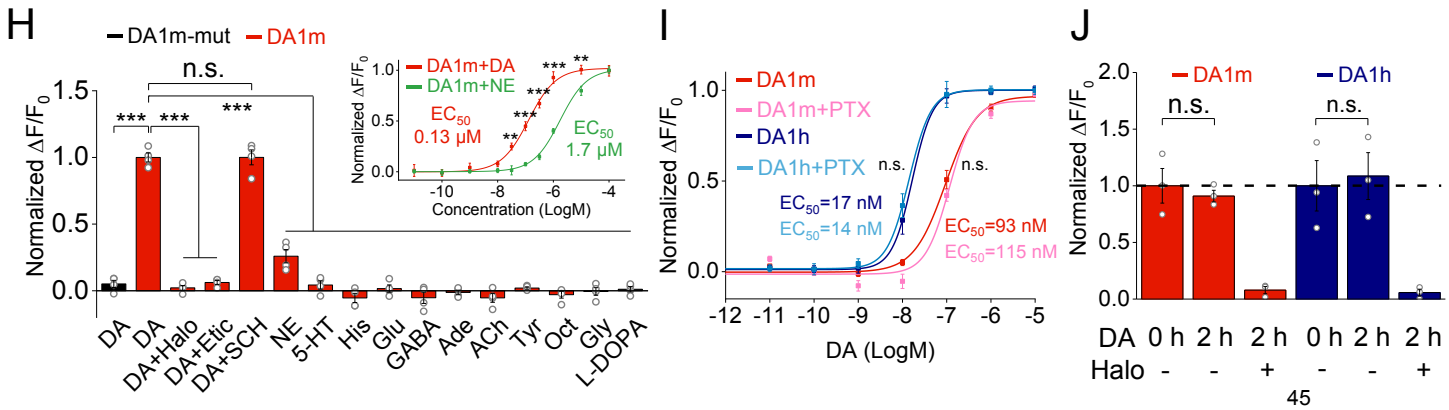

Figure 2

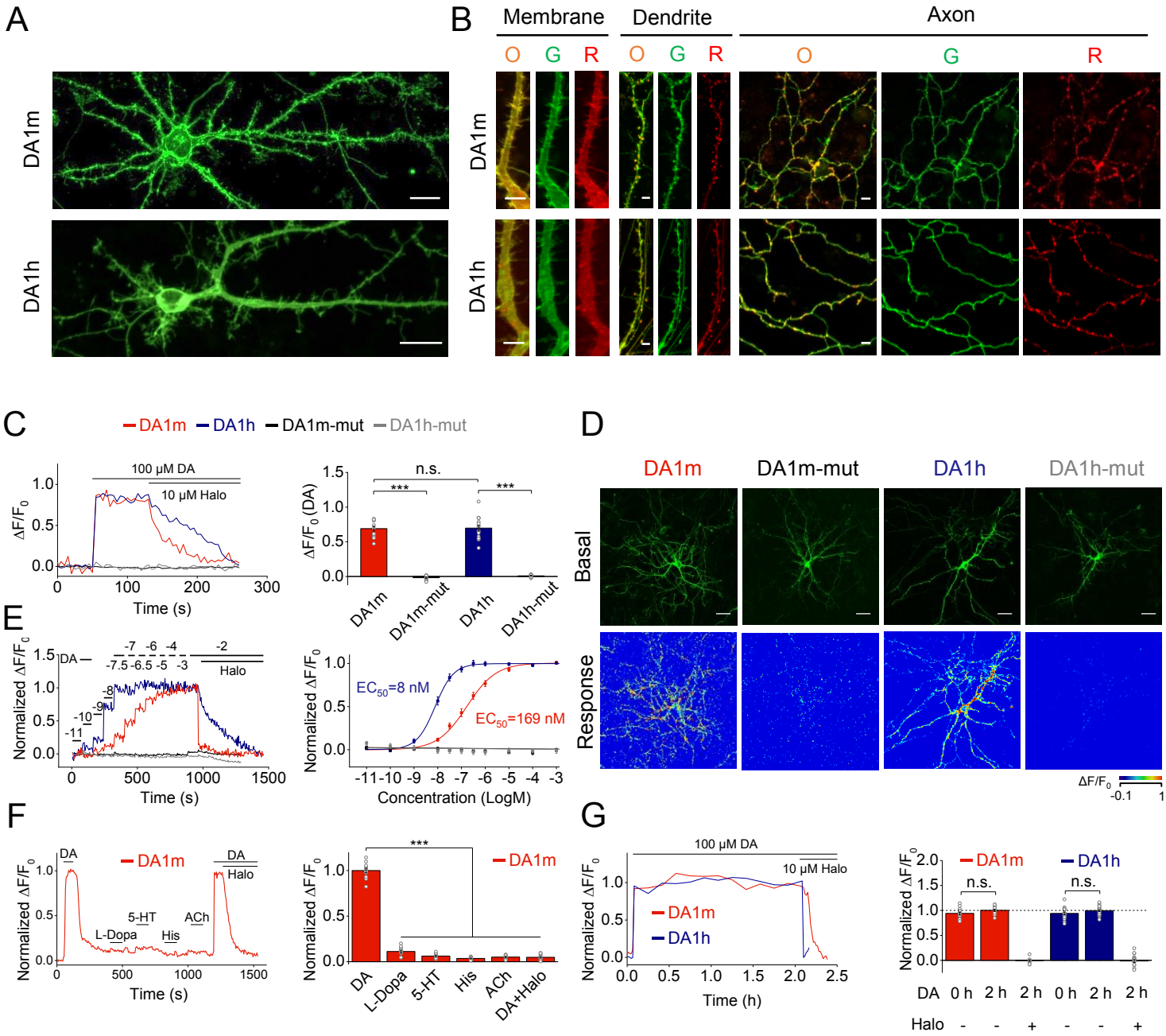

Figure 3

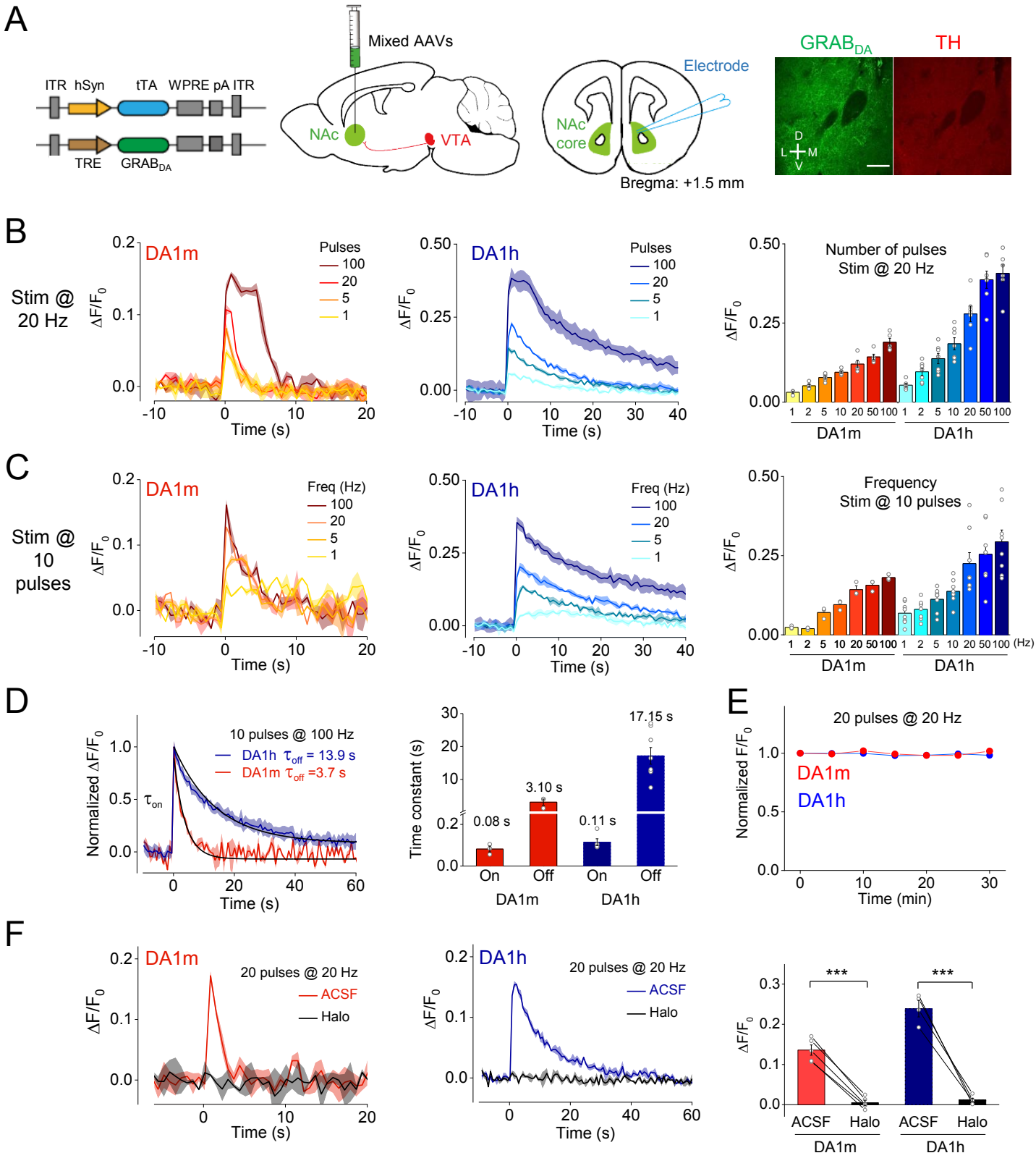

Figure 4

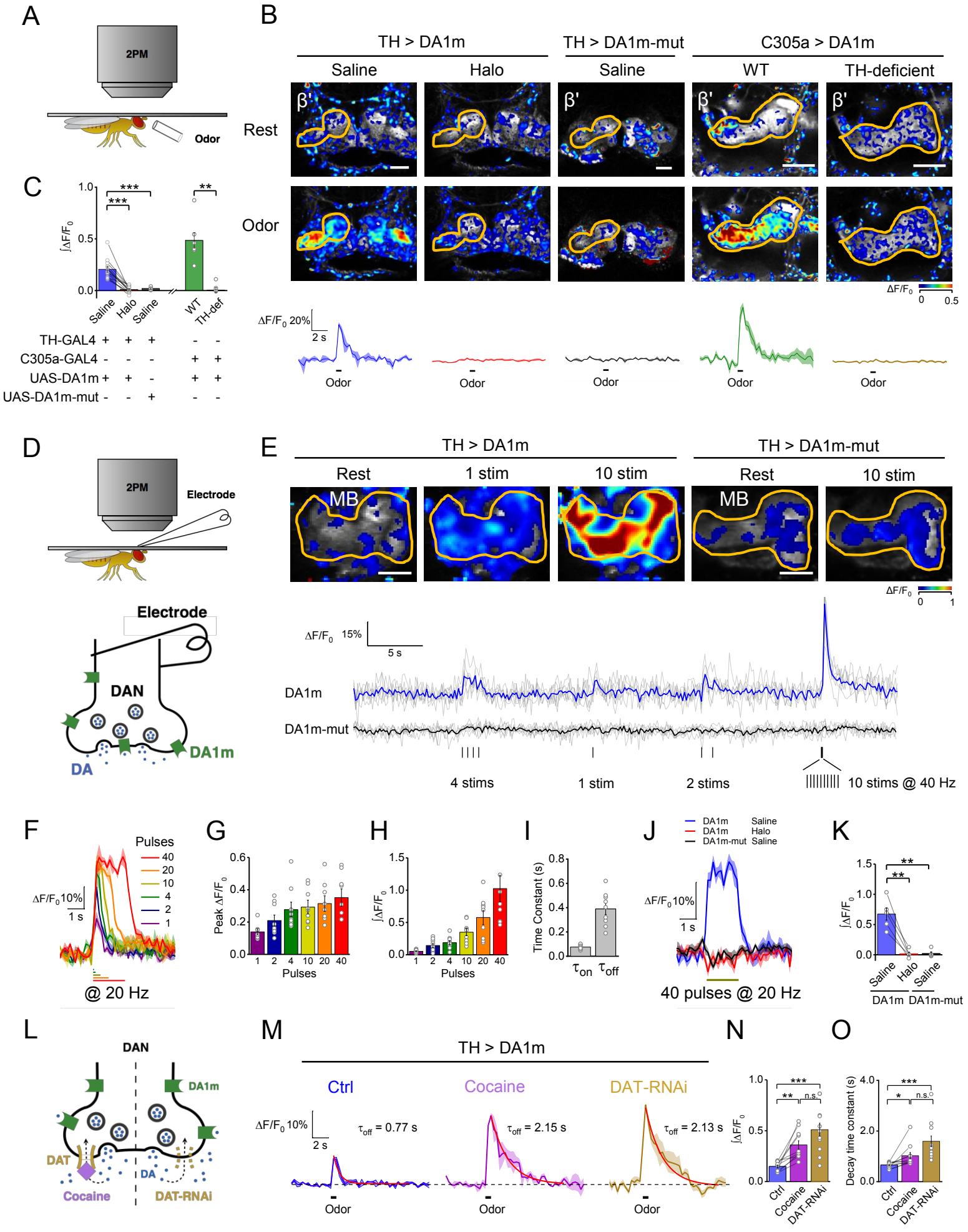

Figure 5

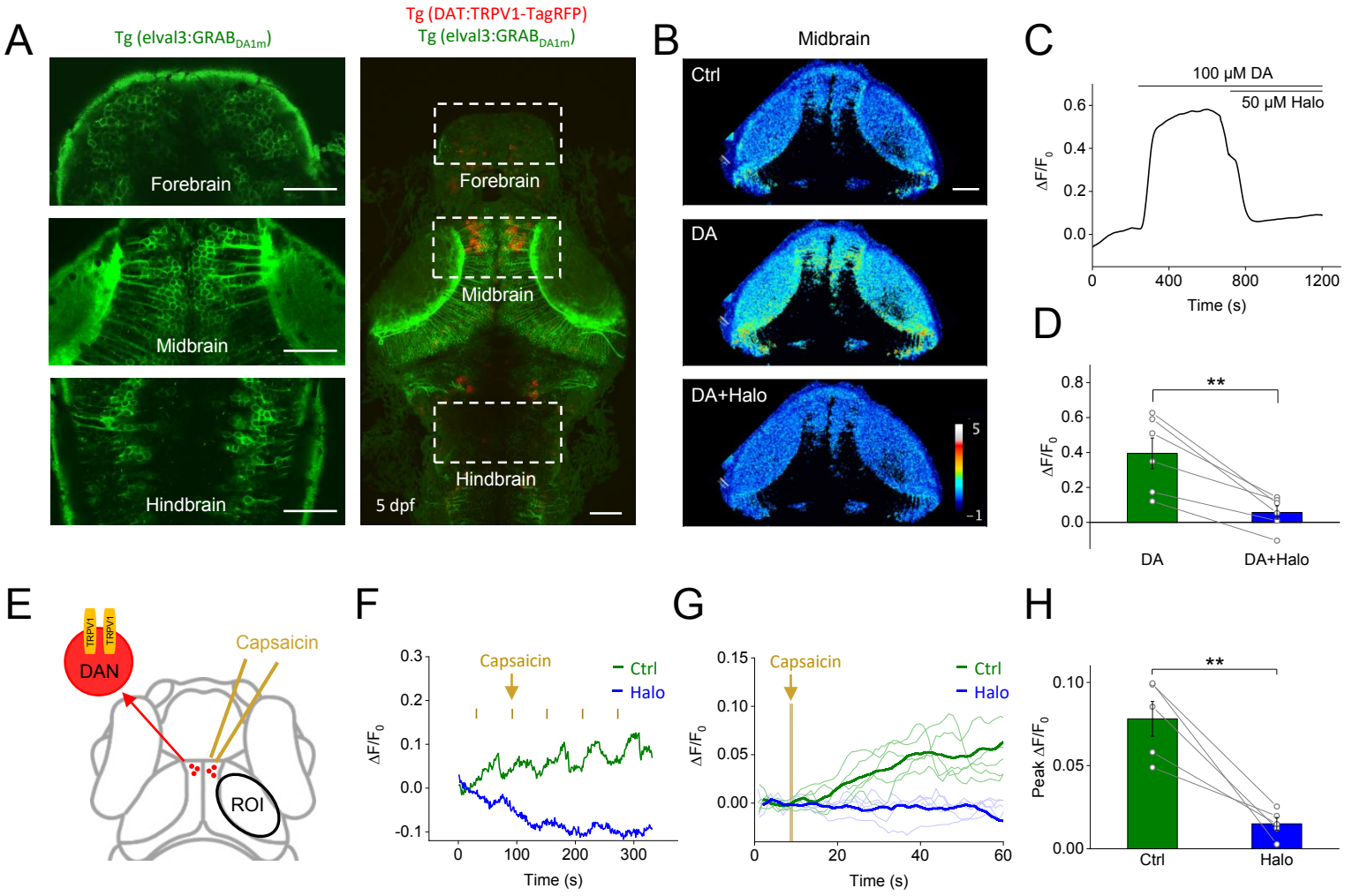

Figure 6

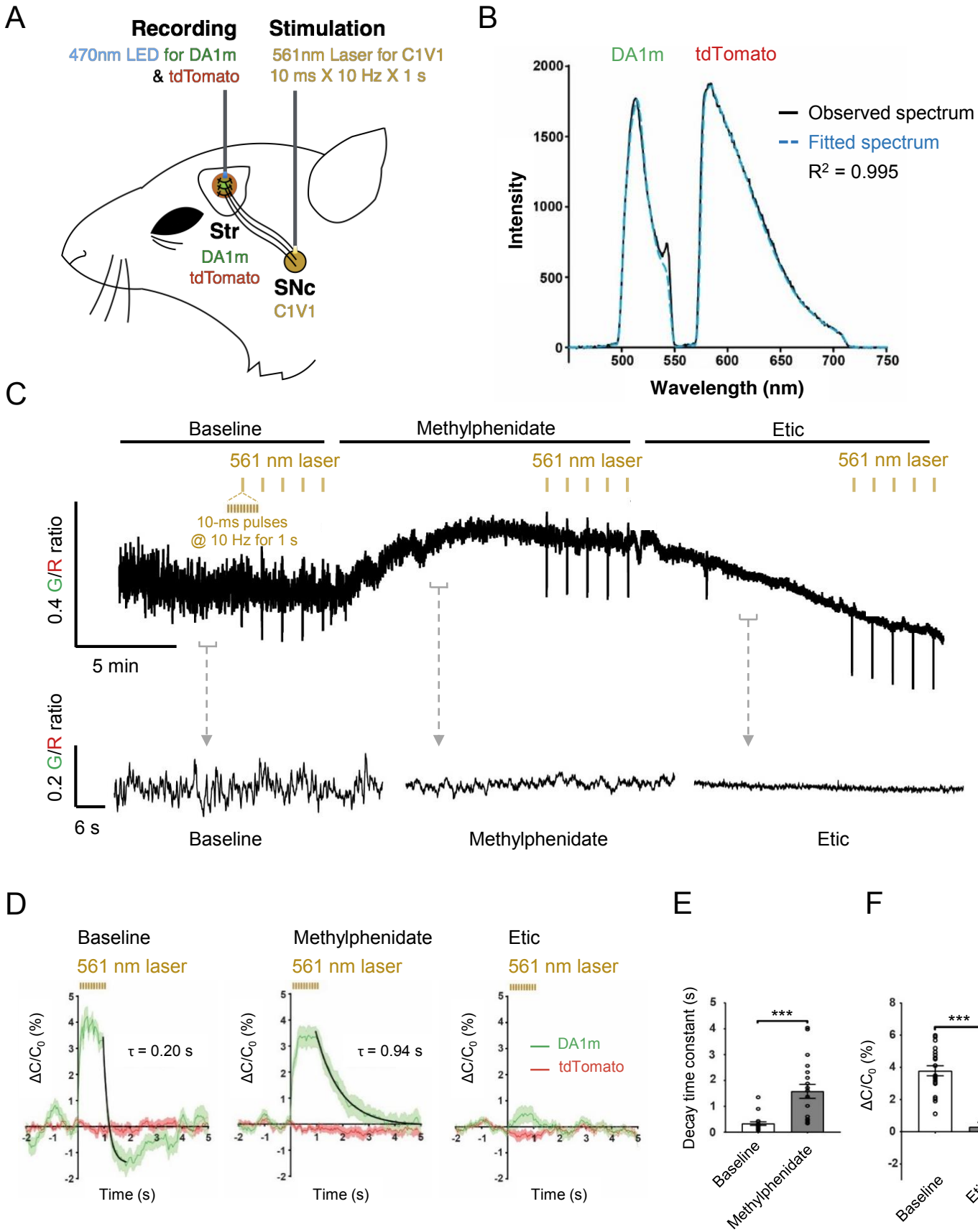

Figure 7

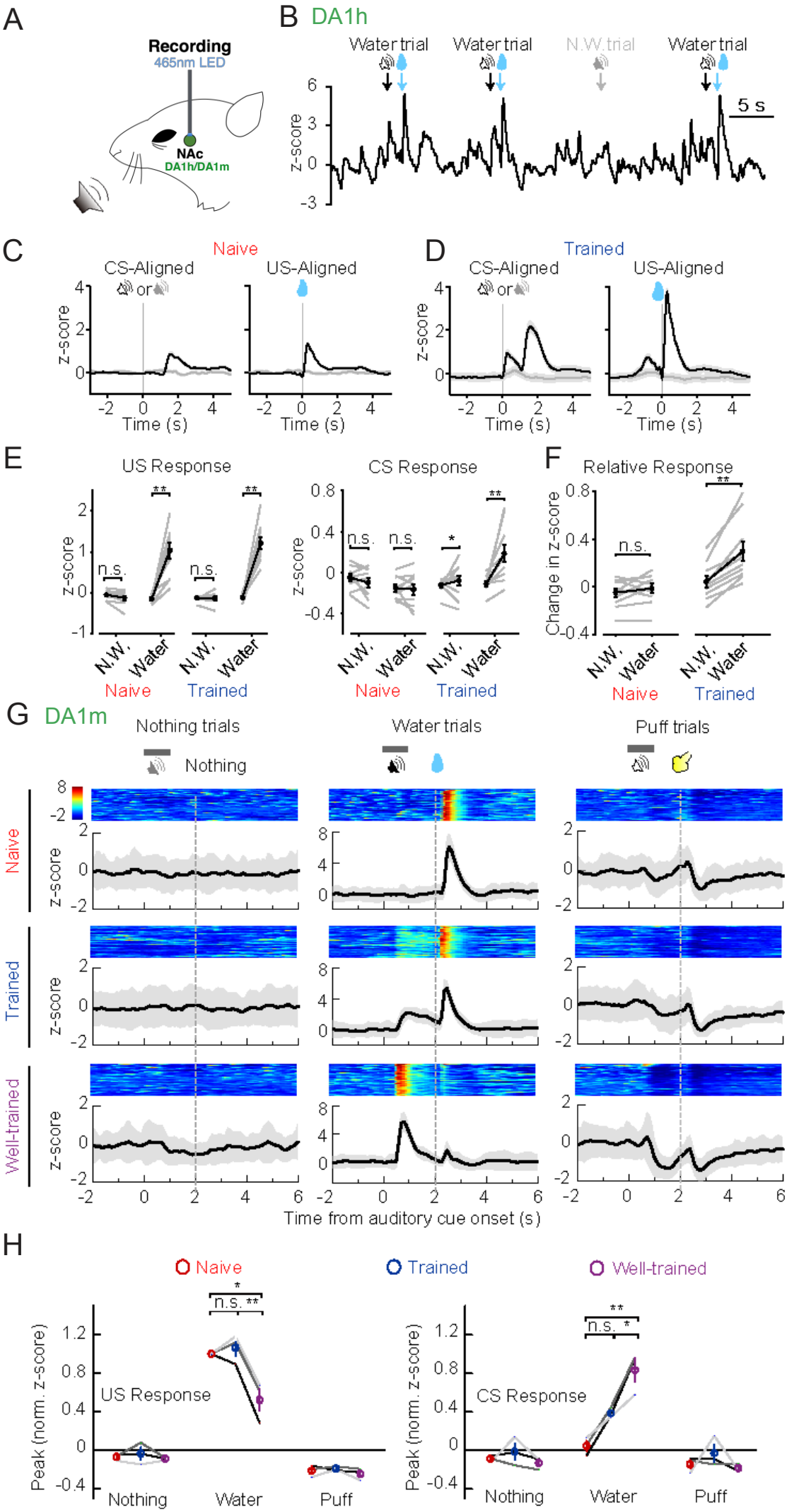

Figure 8

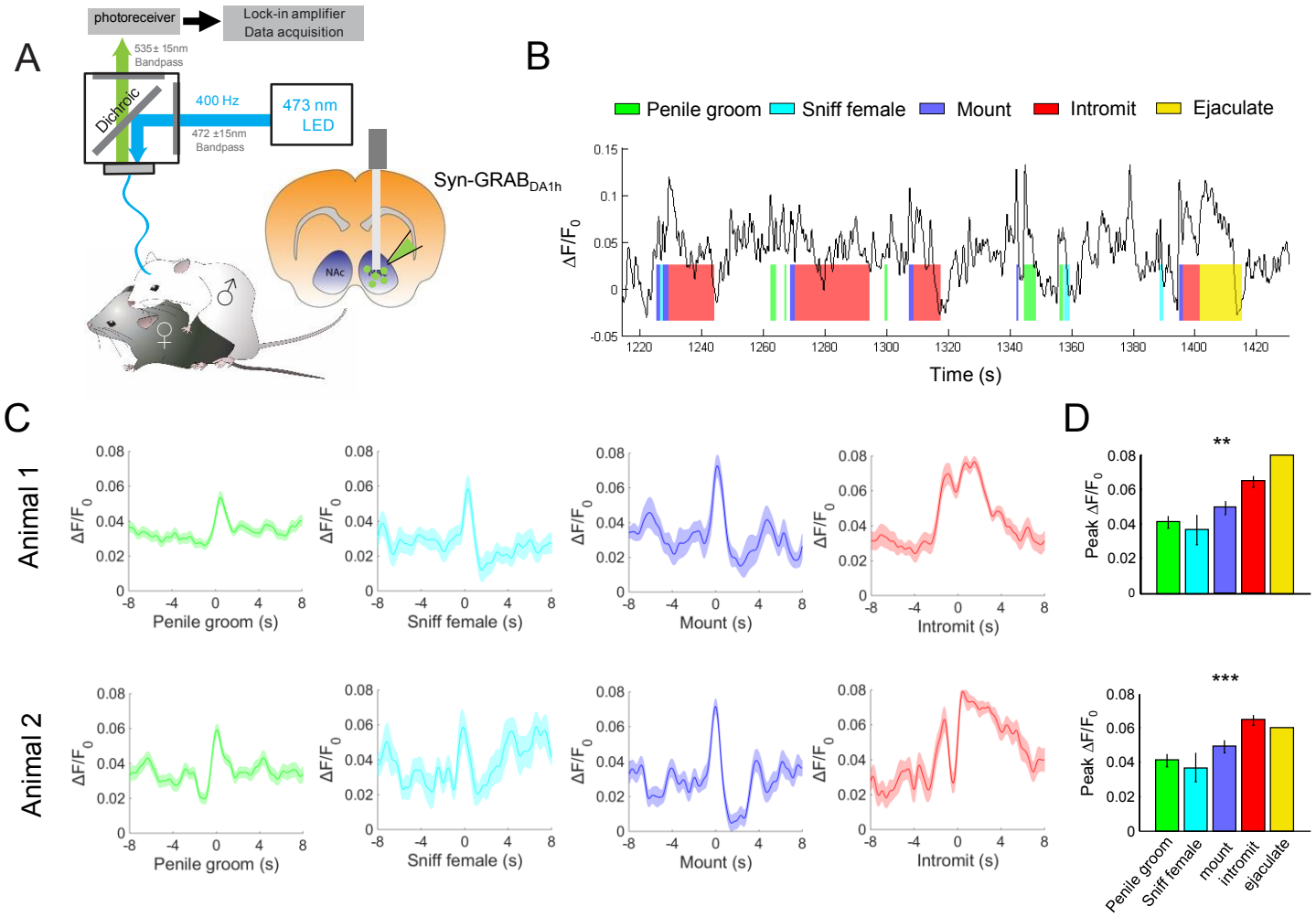

Figure S1: Comparison of DRs and DR-based chimeras, related to Fig. 1.

(A) The fluorescence and membrane trafficking of all five DRs with cpEGFP insertion. A membrane localized RFP (RFP-CAAX) was co-expressed to indicate the plasma membrane and EGFP-CAAX was set as a control. Left, the fluorescence images of HEK293T cells expressing all five DR-based chimeras (green) and RFP-CAAX (red). Middle, the normalized line-scanning plots of the fluorescence signals in both green and red channels. Right, Pearson colocalization ratios between the DR-based chimeras and RFP-CAAX (n = 30/2 for each protein; $p < 0.001$ comparing D_2R with D_3R, D_4R and D_5R; $p = 0.001$ between D_2R and EGFP-CAAX; $p = 0.006$ between D_2R and D_1R).

(B) DA binding affinities of five subtypes of DRs.

(C) Similar as (A), except different D_2R based $GRAB_{DA}$ sensors were characterized, including $GRAB_{DA1m}$, $GRAB_{DA1m\text{-}mut}$, $GRAB_{DA1h}$, $GRAB_{DA1h\text{-}mut}$ and Golgi marker KDELR1-GFP as a control (n = 30/2 for each protein; $p > 0.05$ among $GRAB_{DA}$ sensors; $p < 0.001$ comparing KDELR1 with $GRAB_{DA}$ sensors).

(D) Sequence alignment of the binding pockets of D_1R-D_5R and D_2R-based $GRAB_{DA}$ sensors. Two blue-shaded amino acids indicate C118A and S193N mutation sites.

Scale bars in (A) and (C), 10 μm.

Figure S2: Photostability of $GRAB_{DA1m}$ and $GRAB_{DA1h}$ compared with other fluorescent probes, related to Fig. 1.

(A) Representative photobleaching curves of $GRAB_{DA1m}$, $GRAB_{DA1h}$, EGFP-CAAX and iGluSnFR expressed in HEK293T cells under confocal imaging (488 nm laser with ~350 μW intensity).

(B) The group data of fluorescence decrease time constants of $GRAB_{DA1m}$, $GRAB_{DA1h}$, EGFP-CAAX and iGluSnFR (n = 10/3; p = 0.350 between $GRAB_{DA1m}$ and $GRAB_{DA1h}$; $p < 0.001$ comparing $GRAB_{DA1m}$ with EGFP-CAAX and iGluSnFR).

Figure S3: The selectivity of GRAB$_{DA1h}$, related to Fig. 1.

Normalized fluorescence responses of GRAB$_{DA1h}$- or GRAB$_{DA1h-mut}$-expressing cells to the application of 1 μM different compounds, including: DA, DA with Halo, DA with Etic, DA with SCH, 5-HT, His, Glu, GABA, Ade, ACh, Tyr, Oct, Gly and L-Dopa (the first bar shows GRAB$_{DA1h-mut}$-expressing cells in response to DA; n = 3 wells with each well of 200-400 cells; p < 0.001 for DA-induced responses between GRAB$_{DA1h}$ and GRAB$_{DA1h-mut}$; p = 0.66 for GRAB$_{DA1h}$ responses induced by DA comparing with DA+SCH; p = 0.037 for GRAB$_{DA1h}$ responses induced by DA comparing with NE; p < 0.001 for GRAB$_{DA1m}$ responses induced by DA comparing with DA+Halo, DA+Etic, 5-HT, His, Glu, GABA, Ade, ACh, Tyr, Oct, Gly and L-DOPA). The inset, normalized dose-dependent fluorescence responses of GRAB$_{DA1h}$-expressing cells to the application of DA (blue) or NE (orange) (n = 6 wells with each well of 200-400 cells; p < 0.001 at -8, -7.5, -7 and -6.5; p = 0.049 at -6).

Figure S4: Expression and membrane trafficking of GRAB$_{DA1m-mut}$ and GRAB$_{DA1h-mut}$ in cultured neurons, related to Fig. 1.

The fluorescence images of GRAB$_{DA1m-mut}$- and GRAB$_{DA1h-mut}$-expressing neurons under confocal microscope. RFP-CAAX was co-expressed in the same neuron to indicate the plasma membrane. Scale bars of whole views, 20 μm. Scale bars of zoom-in views, 5 μm.

Figure S5: $GRAB_{DA1m}$ expression has no effect on the odor-evoked Ca^{2+} signaling, related to Fig. 4.

(A) The schematic of *in vivo* olfactory stimulation experiment under two-photon microscope.

(B) Representative pseudo-color images and traces of fluorescence responses of jRCaMP1a-exprssing DANs (left) or Kenyon cells (right) to 1 s olfactory stimulation. Traces are 3-trial-averaged results from one fly, and are shaded with ± SEM. Scale bars, 25 μm.

(C) The integrals of jRCaMP1a signals are summarized. Each dot represents data from one fly (TH > jRCaMP1a: n = 10 flies; TH > jRCaMP1a, $GRAB_{DA1m}$: n = 11 flies; 30y > jRCaMP1a: 11 flies; 30y > jRCaMP1a, $GRAB_{DA1m}$: n = 12 flies; p = 0.503 between TH > jRCaMP1a and TH > jRCaMP1a, $GRAB_{DA1m}$; p = 0.097 between 30y > jRCaMP1a between 30y > jRCaMP1a, $GRAB_{DA1m}$). Error bars, ± SEM. Student's t-test is performed; n.s., not significant.

Figure S1

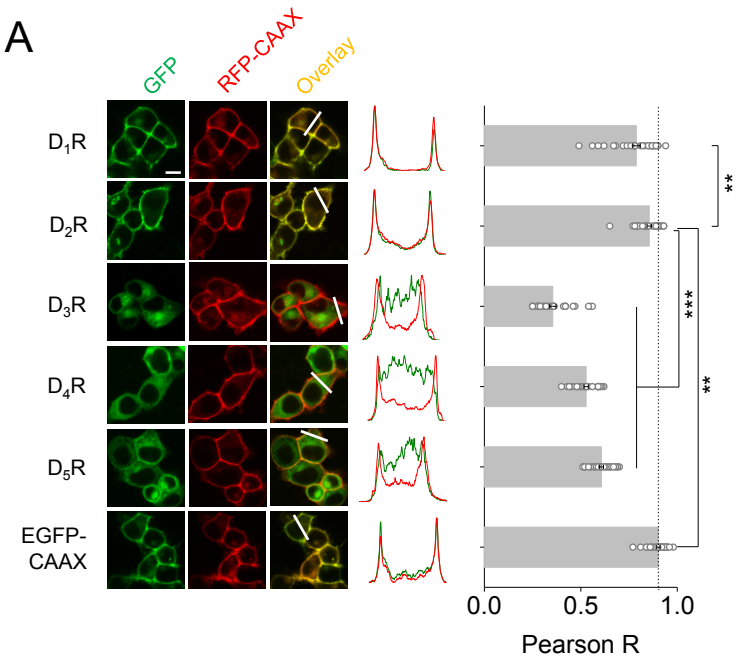

B

Receptor	pK_i	Ref
D_1R	4.3-5.6	Sunahara et al., 1991 Tiberi and Caron, 1994
D_2R	4.7-7.2	Schetz et al., 2000 Sokoloff et al., 1990
D_3R	6.4-7.3	Burris et al., 1995 Freedman et al., 1994 Sautel et al., 1995 Sokoloff et al., 1990
D_4R	7.6	Schetz et al., 2000
D_5R	6.6	Sunahara et al., 1991

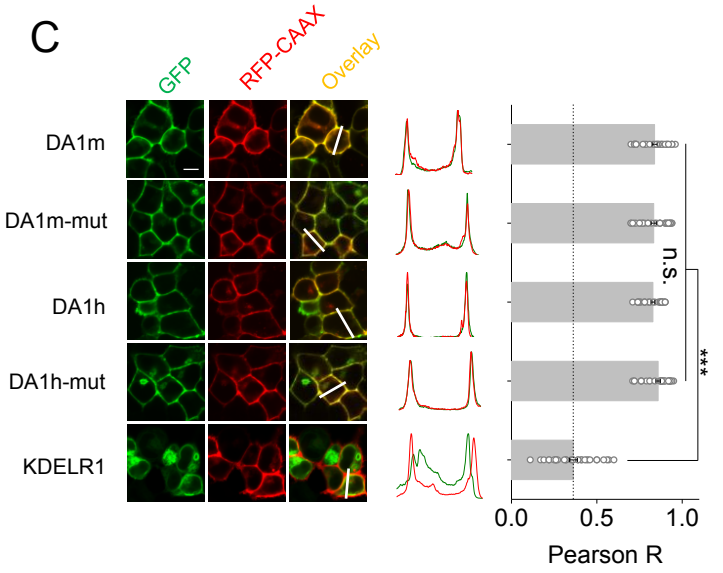

D

	2.61	3.28	3.32	3.33	3.36	3.37	5.39	5.42	5.43	6.48	5.46	6.51	6.52	6.55	6.56	7.35	7.39	7.43
D_1R	K	W	D	I	S	S	A	S	S	S	W	F	F	N	C	Y	N	W
D_3R	V	F	D	V	C	I	V	S	S	S	W	F	F	H	V	Y	T	Y
D_4R	F	L	D	V	C	L	V	S	S	S	W	F	F	H	I	V	T	Y
D_5R	K	W	D	I	S	S	A	S	S	S	W	F	F	N	C	F	V	W
$D_2R/GRAB_{DA}$	V	F	D	V	C	I	V	S	S	S	W	F	F	H	I	Y	T	Y
$GRAB_{DA\text{-}mut}$	V	F	D	V	A	I	V	N	S	S	W	F	F	H	I	Y	T	Y

Figure S2

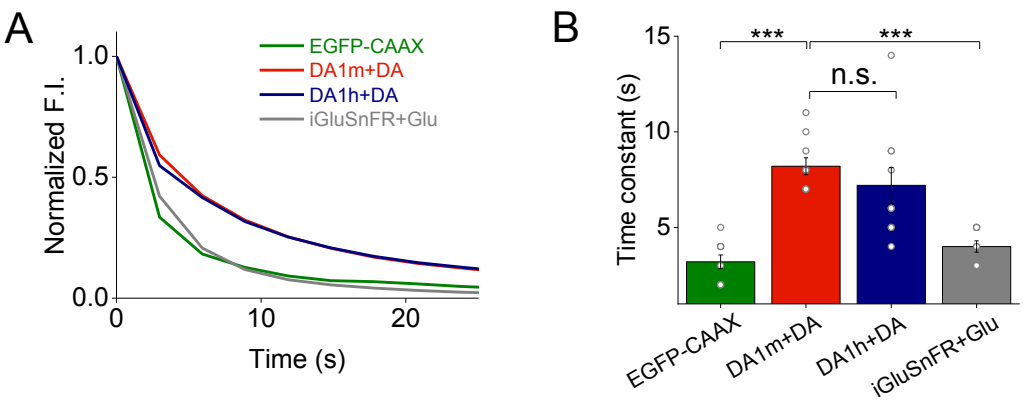

Figure S3

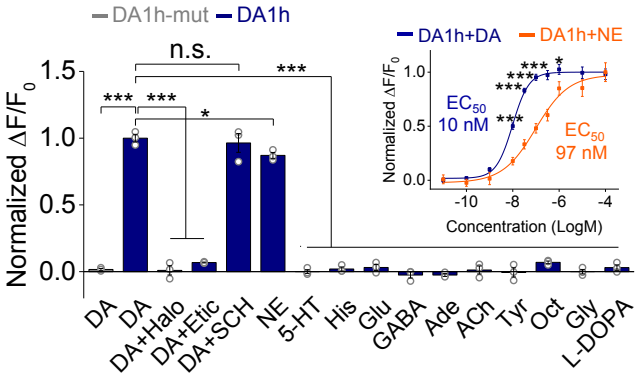

Figure S4

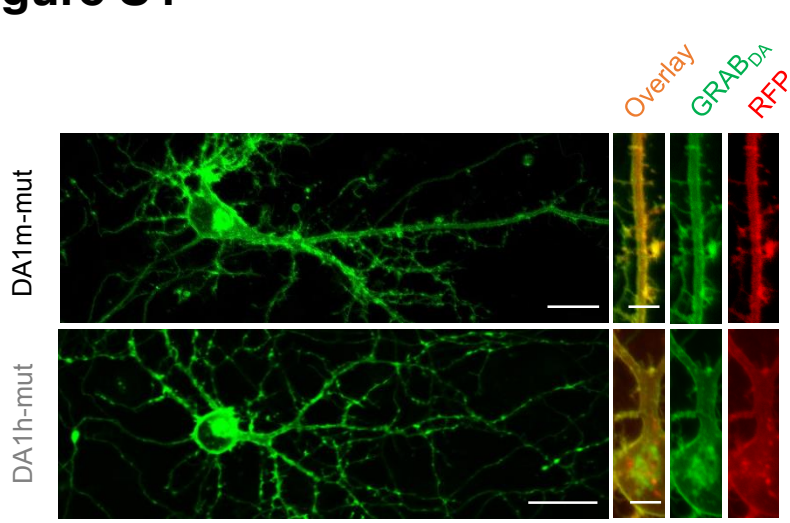

Figure S5